C.P. No. 1024

C.P. No. 1024

MINISTRY OF TECHNOLOGY

AERONAUTICAL RESEARCH COUNCIL

CURRENT PAPERS

An Investigation of Stress Redistribution Caused by Creep in a Thick-Walled Circular Cylinder Subjected to Axial and Thermal Loading

By

J. M. Clarke

LONDON: HER MAJESTY'S STATIONERY OFFICE

1969

TEN SHILLINGS NET

U.D.C. No. 539.434:539.319

C.P. No. 1024*

June 1967

An investigation of stress redistribution caused by creep in a thick-walled circular cylinder subjected to axial and thermal loading

- by -

J. M. Clarke

SUMMARY

A thick-walled tube was subjected to an axial load and a radial temperature distribution which caused thermal stresses. The creep strains and the eventual rupture times were observed and compared with conventional creep tests and theoretical analysis. Theory suggested and experiments confirmed that stress redistribution caused the overall strain behaviour to approach that for the mean axial stress and the mean radial temperature.

Description of the experimental technique and apparatus includes a novel and simple optical extensometer. Appendices contain a complete analytic treatment of the triaxial stress problem in a long thick tube in the presence of an arbitrary distribution of non-elastic strains, and a treatment of some conditions under which stress-redistribution calculations can lead to a "steady state" or "fully redistributed" stress pattern.

A less rigorous theoretical treatment which ignores radial constraints is shown to lead to an under-estimate of the thermal stresses and of the time required for stress redistribution to occur.

---

* Replaces N.G.T.E. R289 - A.R.C.29 484

CONTENTS

TABLES

APPENDICES

ILLUSTRATIONS

ILLUSTRATIONS (cont'd)

1.0 Introduction

The application of the digital computer to stress analysis allows solutions to be obtained easily to a large number of problems which have to be tackled by numerical methods. One example is the redistribution of stress in an internally cooled gas turbine rotor blade[1]. This redistribution is caused by the accumulation of creep strains at different rates which depend on the temperature, stress and previous history of each element of the blade. The most important result of the stress redistribution process is that the stress pattern becomes more uniform than that calculated simply on a basis of the thermal strains and a perfectly elastic material. This is illustrated for a very simple tensile system on Figure 1. By consideration of rupture times based on the most severe conditions of stress and temperature within a blade the stress pattern can be shown to become more favourable as redistribution proceeds; furthermore the redistribution is predicted to be complete before any part of the blade would be expected to fail. The time to rupture of the blade should therefore be more closely related to the mean stress and mean temperature at a spanwise position than to the most severe combination of stress and temperature at the beginning of redistribution.

In order to obtain some guidance to the validity of the assumptions and to compare the predicted rupture life with that actually observed, an experimental and theoretical investigation has been conducted on a thick-walled circular cylinder subjected to an axial tensile load and a radial temperature gradient. Apart from being worthy of study in its own right, the choice of a cylindrical geometry made the problem amenable to analysis while corresponding closely to the geometrically more complex situation within a cooled turbine rotor blade. It also enabled an experiment to be conducted under carefully controlled laboratory conditions and strain measurements to be taken. Confirmation that the accumulation of axial creep strain and the observed rupture lives agree well with those based on the conditions of mean stress and temperature are the most important results from this experimental investigation.

Figure 2 shows a schematic arrangement of the apparatus used. The axial load was applied by a 5-ton Denison creep machine and the radial temperature gradient was produced by passing an electrical current axially along the test specimen and allowing the latter to radiate freely from its outside surface. A number of experiments were repeated to determine scatter and some control experiments were made to separate variables, the whole programme involving about 5000 hr of creep testing.

2.0 Experimental

2.1 Design of the experiment

The dimensions, temperatures and stresses used for the experiment were chosen to satisfy,

(i) a modest electric power requirement

(ii) tight manufacturing tolerances, especially in the bore of the test specimen

(iii) mean stress and temperature sufficient to cause rupture in about 400 hr if redistribution occurred

(iv) a combination of local stress and temperature severe enough to initiate rupture in a much shorter time if redistribution did not occur

(v) the temperature to be high enough to cause the required radiation intensity from the outside surface.

A number of exploratory calculations using manufacturer's data for Nimonic alloy 105 led to the choice of the following values:-

tube length	3 in.
inside diameter	$\frac{5}{16}$ in.
outside diameter	$\frac{5}{8}$ in.
mean axial stress	4 ton/in^2
maximum axial stress	7 ton/in^2
mean temperature	950°C

For these conditions the rupture times for the most severe (initial) stress and temperature and the mean stress and temperature were estimated to be 40 hr and 400 hr respectively. The calculations showed that there was very little freedom to depart from the chosen values.

The tests on tubular specimens containing a radial temperature gradient (Type 1 tests) were supported by four other test arrangements intended to act as controls and to provide creep data for the same batch of material. They are shown on Figure 3.

Type 2 tests simulated Type 1 except for the provision of external insulation and an auxiliary heater to ensure a uniform radial temperature. These tests were therefore free from thermal stresses.

The single Type 3 test also used a tubular specimen but heated it in a conventional creep test furnace.

Type 4 and 5 tests used solid cylindrical specimens of two different types to establish the creep strain behaviour of the material. The test technique conformed with orthodox creep test methods.

2.2 Control and measurement of temperature

The temperature sensitivity of rupture times, at the chosen mean stress and temperature levels, was 4·5 per cent reduction in life per ^{o}C rise in temperature. The temperature of the furnace heated specimens was generally controlled within $\pm\frac{1}{2}^{o}C$ and that of the tube tests within approximately $\pm 1^{o}C$. Platinum resistance thermometers were used as sensors for the proportional temperature controllers but temperature measurements were made using platinum/platinum rhodium thermocouples. For the radiating tube tests three such thermocouples were lightly welded to the bore, and for the others the thermocouples were tied to the specimen surface and shielded against direct radiation from the furnace walls. The temperature difference between inside and outside surfaces of the tube was calculated using the measured electrical power and the manufacturer's data for thermal conductivity.

2.3 Development of the apparatus

The calculation of temperature difference referred to in the last section assumed no loss of heat from the gauge length (the central $\frac{5}{8}$ in.) by conduction along the tube axis. It was therefore necessary to ensure a uniform temperature for about an inch in the centre of the tube length. This was achieved, after some abortive attempts with auxiliary end heaters, by providing insulating collars at the ends as shown in Figure 4. These collars reduced radiant heat loss in the areas where conduction was causing lower temperatures. Figure 5 shows the longitudinal temperature profiles obtained under various conditions. Preliminary creep tests showed the material to be considerably stronger than the manufacturer's data implied and for this reason the test temperatures were raised by $20^{o}C$ to return the rupture times to the values originally intended.

2.4 Measurement of strain

It was felt desirable to measure strains on the radiating specimens if this could be done without interfering with the symmetry of heat flux. For this purpose a simple and novel optical extensometer was constructed (see Figure 6).

The principle employed was the displacement of a light path by the interposition of inclined glass blocks as shown on Figure 7. One pair of fixed blocks served to superimpose the images while a second pair of thinner blocks was rotated to accommodate and measure strains. When used to observe an object illuminated by white light it was necessary to insert a dark red filter to reduce diffraction effects but when observing a red-hot specimen this was not so critical.

During the experiment both diametral and longitudinal strains were measured by simply rotating the instrument about its optical axis. The gauge length for diametral strain was defined clearly by the edges of the tube, and two circumferential platinum wires were lightly welded to the outside of the tube $\frac{5}{8}$ in. apart to define the axial gauge length. It was found that resolution was limited by clarity of the objects observed and could have been improved by using small bright sources of additional illumination (preferably monochromatic).

Because the position of coincidence of the two images in the telescope eye-piece required judgement several readings (usually three) were taken on each occasion. Best fitting curves of strain versus time were obtained by using the fourth order polynomial with the least sum of the squares of the errors. Subsequently histograms were constructed of the errors relative to these curves and it was found that the 50 per cent certainty band had width about ±0·025 per cent for the diametral strains and ±0·050 per cent for the axial strains. The former was more accurate because the gauge length was more clearly defined. These values are maximum values because they include not only instrument errors but also errors due to the fitted curve being too smooth and therefore possibly masking real effects.

In order to measure the strains during the Type 4 tests, use was made of transducers attached to a design of extensometer described in Reference 3 and widely used at N.G.T.E.

2.5 Results

The results for individual tests are distinguished by code letters. The key to these letters is given on Figure 21 which folds out for use with Figures 8, 9, 12 and 13. Comments on the results are postponed until Section 4.0.

2.5.1 Rupture times and reductions of area

The rupture times and reductions of area are given in Table I together with the test conditions. The same rupture time information is shown graphically on Figures 8 and 9 with the temperatures measured by the thermocouple nearest to the eventual rupture line.

2.5.2 Strain records

Only two strain records were obtained from the three Type 1 tests because the first was completed before the construction of the optical extensometer. Figures 10 and 11 show the results. For the small strains the scale has been magnified. The short vertical lines on the figures show the range between the greatest and least strains measured on each occasion.

Type 2 tests were enclosed by lagging so that strain measurement using the optical extensometer was not possible.

Figures 12 and 13 show the creep strain readings for the Type 4 and 5 tests at the two different conditions of stress and temperature.

2.5.3 Micrographs

Micrographic sections were taken off several specimens and three of these are shown in Figures 14 and 15. Figure 14 from specimen C illustrates the typical creep type rupture caused by cracking at the grain boundaries. There are no obvious peculiarities attributable to the electrical heating technique.

Figure 15 confirms a difference between the inside and outside conditions in Test C. It shows more extensive oxidation on the inside surface; indeed this surface of C was more severely attacked than any other.

3.0 Theoretical

3.1 Some order of magnitude considerations

Using manufacturer's data for Nimonic alloy 105 at 970°C it may be shown that a strain of 0·06 per cent may be caused by:-

either	elastic strain from a uniaxial stress of 5 ton/in^2
or	creep strain after about 5 hr at 5 ton/in^2
or	a temperature difference of 15°C.

The equal strains caused by the conditions listed above, all of which are fairly easily realised, show that the behaviour of a hot component is typified by a strong interaction between elastic, thermal expansion and creep effects. At lower temperatures it would also be necessary to consider plastic flow.

3.2 Stress analysis

The elastic thermal stress analysis of a long thick cylinder is available from standard texts[4] for an arbitrary radial temperature distribution. The temperature influences the stress pattern by introducing thermal strains. Whereas thermal strains are concerned with volume changes, creep strains are concerned with shape changes and it was therefore necessary to extend the solution. Appendix II gives details of the extended analysis. The approach is analytical rather than numerical but completely closed forms of solution for the stresses are obtainable only if analytic functions are assumed for the distributions of the various non-elastic strains. In practice these distributions were represented by arrays of numbers within a digital computer and the accuracy of solution then depends on the extent of these arrays and the numerical method used for their integration.

The stress analysis does not need to distinguish the various (e.g., thermal, plastic, creep) components of non-elastic strain and the procedure adopted in the theoretical work described here was to add together the terms caused by thermal expansion and creep at any instant prior to the calculation of the corresponding stress pattern. Implicit assumptions in the analysis are that the non-elastic strains should be small enough to permit the usual tensor representation and that the principal directions of non-elastic strain must coincide with those of the elastic stresses and strains, namely the hoop radial and axial directions. Furthermore, the material is assumed to be elastically and plastically isotropic.

3.3 Calculation of creep strain increments

Creep behaviour is still described in empirical terms and comprehensive results from creep tests of materials such as nickel base alloys are only available for tests at constant stress and temperature under uniaxial tensile conditions. In stress redistribution studies, involving a

changing pattern of multiaxial stresses, it is necessary therefore to augment the data by using certain hypotheses in order to

(a) permit estimates of behaviour under changing uniaxial conditions and

(b) permit predictions of behaviour under multiaxial stress situations including compression.

The hypotheses used in the work described here are not new and are reproduced here simply for completeness.

3.3.1 Time and strain hardening hypotheses

These are two of the many alternative hypotheses currently being considered. For more complete descriptions of them see for instance References 5, 6, 7, 8 and 9.

Suppose creep strain data from tests at constant stress and temperature are available in the form

$$\varepsilon = f(\sigma, T, t) \qquad \ldots.(1)$$

where ε is creep strain

σ is stress (uniaxial tensile)

T is temperature

t is time measured from application of the load

f is a function with σ, T and t as variables

then in principle the same information can also be expressed as

$$t = g(\sigma, T, \varepsilon) \qquad \ldots.(2)$$

where g is a different function.

According to the "time hardening" hypothesis the increment of creep strain caused by a period (Δt) of constant stress (σ_1) and temperature (T_1) following the instant at which the strain was ε_1 and the time was t_1 is given by

$$\Delta\varepsilon_t = f(\sigma_1, T_1, t_1 + \Delta t) - f(\sigma_1, T_1, t_1)$$

$$= f_t(\sigma_1, T_1, t_1, \Delta t) \qquad \ldots.(3)$$

where the subscript t refers to time hardening.

According to the "strain hardening" hypothesis the increment of creep strain caused by the same conditions would be

$$\Delta\varepsilon_s = f\Big(\sigma_1, T_1, g(\sigma_1, T_1, \varepsilon_1) + \Delta t\Big) - \varepsilon_1$$

$$= f_s(\sigma_1, T_1, \varepsilon_1, \Delta t) \qquad \ldots\ldots(4)$$

where the subscript s refers to strain hardening.

It is apparent that the influence of previous loading and straining is being introduced by the single values of time (t_1) and strain (ε_1) respectively, and a convenient (non-iterative) use of the strain hardening hypothesis depends on the existence of both "f" and "g" functions. Suitable expressions are given in Reference 10. It should be noted that many forms of "f", for example sums of terms containing powers of t, do not lend themselves to conversion to "g" functions.

3.3.2 Effective stress and strain

The expressions (3) and (4) above which refer to uniaxial tensile data can be extended to multiaxial situations by postulating effective stresses ($\bar{\sigma}$) and strains ($\bar{\varepsilon}$) so that

$$\Delta\bar{\varepsilon}_t = f_t(\bar{\sigma}_1, T_1, t_1, \Delta t) \qquad \ldots\ldots(5)$$

$$\Delta\bar{\varepsilon}_s = f_s(\bar{\sigma}_1, T_1, \bar{\varepsilon}_1, \Delta t) \qquad \ldots\ldots(6)$$

where $\bar{\varepsilon}$, $\Delta\bar{\varepsilon}$ and $\bar{\sigma}$ are expressed in terms of the principal strains (ε_1, ε_2, ε_3) and principal stresses (σ_1, σ_2, σ_3) by

$$\bar{\varepsilon} = \frac{\sqrt{2}}{3}\sqrt{\Big((\varepsilon_1 - \varepsilon_2)^2 + (\varepsilon_2 - \varepsilon_3)^2 + (\varepsilon_3 - \varepsilon_1)^2\Big)} \qquad \ldots\ldots(7)$$

$$\Delta\bar{\varepsilon} = \frac{\sqrt{2}}{3}\sqrt{\Big((\Delta\varepsilon_1 - \Delta\varepsilon_2)^2 + (\Delta\varepsilon_2 - \Delta\varepsilon_3)^2 + (\Delta\varepsilon_3 - \Delta\varepsilon_1)^2\Big)}$$

$$\ldots\ldots(8)$$

and $$\bar{\sigma} = \frac{1}{\sqrt{2}} \sqrt{\left((\sigma_1 - \sigma_2)^2 + (\sigma_2 - \sigma_3)^2 + (\sigma_3 - \sigma_1)^2 \right)} \qquad \ldots.(9)$$

The multiplying constants being chosen so that for plastic flow under uniaxial stress,

$$\bar{\sigma} = \sigma_1 \qquad \text{when} \quad \sigma_2 = \sigma_3 = 0$$

and $$\bar{\varepsilon} = \varepsilon_1 \qquad \text{when} \quad \varepsilon_2 = \varepsilon_3 = -\tfrac{1}{2}\varepsilon_1 .$$

3.3.3 Levy-Mises flow rule

This concerns the direction of shape change and in its incremental flow form[11,12] it ensures that the increment of effective shear strain corresponds in its direction with the current direction of effective shear stress. It may be stated in the following form,

$$\frac{\sigma_1 - \sigma_2}{\Delta\varepsilon_1 - \Delta\varepsilon_2} = \frac{\sigma_2 - \sigma_3}{\Delta\varepsilon_2 - \Delta\varepsilon_3} = \frac{\sigma_3 - \sigma_1}{\Delta\varepsilon_3 - \Delta\varepsilon_1} \qquad \ldots.(10)$$

It follows from the definitions of effective stress and strain that the ratio in Equation (10) also equals $2\bar{\sigma}/3\Delta\bar{\varepsilon}$.

3.3.4 Constant volume condition

Equations (5) or (6) with (7), (8), (9) and (10) suffice to determine differences between strain increments in the principal directions. In order to determine completely the actual values a further condition is required and this is taken to be the constant volume condition,

$$\Delta\varepsilon_1 + \Delta\varepsilon_2 + \Delta\varepsilon_3 = 0 \qquad \ldots.(11)$$

Simultaneous use of the above conditions is assured by calculating strain increments using the following expressions

$$\left.\begin{aligned} \Delta\varepsilon_1 &= \frac{\Delta\bar{\varepsilon}}{2\bar{\sigma}} (2\sigma_1 - \sigma_2 - \sigma_3) \\ \Delta\varepsilon_2 &= \frac{\Delta\bar{\varepsilon}}{2\bar{\sigma}} (2\sigma_2 - \sigma_1 - \sigma_3) \\ \Delta\varepsilon_3 &= \frac{\Delta\bar{\varepsilon}}{2\bar{\sigma}} (2\sigma_3 - \sigma_2 - \sigma_1) \end{aligned}\right\} \qquad \ldots.(12)$$

3.4 Representation of creep properties

The formulae adopted here for the description of creep properties (as measured during conventional creep strain tests at constant tensile stress and temperature) were developed in 1963 for use in the calculation of stress redistribution effects in cooled gas turbine blades, and have been found to provide an accurate and convenient method for all the Nimonic alloys[10]. They have the particular advantage which is unusual in formulae used for this purpose that while permitting a representation of both primary and tertiary creep they allow explicit evaluation of strain from time and also time from strain. The desirability of this feature was mentioned in Section 3.3.1 in connection with the use of the strain hardening hypothesis.

3.5 Evaluation of creep properties from experimental data

Because the experimental programme was concerned with a limited number of tests and a relatively small range of stresses and temperatures, it was decided to concentrate on only two different stress/temperature combinations and to do several tests at each to indicate the scatter.

Other more extensive creep strain data for Nimonic alloy 105 were available and were slightly modified in order to comply with the observed strain versus time results for this particular batch.

3.6 Computer program

A program was written in Elliott 803 Autocode to calculate, using either time or strain hardening hypotheses, the redistribution of stresses within a thick tube with non-uniform radial temperature pattern. The loading conditions on the tube are specified by

(i) mean axial stress

(ii) inside and outside pressures (maintained zero in this investigation)

(iii) inside and outside radii

(iv) temperatures at a number of equi-spaced positions through the thickness.

4.0 Discussion of experimental and theoretical results

4.1 Observed rupture times

The rupture time results fall into three categories.

(i) Electrically heated tube specimens, both with and without radial temperature gradients and loaded by a mean axial stress of 4 t.s.i. at a mean temperature of 967·4°C broke after about 500 hr. (Tests A, B, C, D and E.)

(ii) Furnace heated specimens with an axial stress of 4 t.s.i. and a temperature of 970°C broke after about 400 hr. (Tests F, J, K, L and N.)

(iii) Furnace heated specimens with a stress of 7 t.s.i. and a temperature of 965°C broke after about 35 hr. (Tests G, H, I and M.)

4.2 Observed strains

The strain records for the two Type 1 tests shown in Figures 10 and 11 reveal a number of features:-

(i) a very high diametral strain rate at the neck immediately before fracture

(ii) necking occurred on each side of the gauge length

(iii) examination and comparison of the diametral and axial strain rates suggests that there was a volumetric expansion in both tests for approximately the first 100 hr. The magnitude of this effect was much greater for Test B than C but its duration was similar. Subsequently, with the onset of necking (and non-uniform strain in the axial gauge length) the comparison between axial and diametral strains becomes less meaningful. It is of interest to note that Levy[13] has observed an apparent volume increase in the early stages of creep tests on aluminium sheet material.

The strain records for the normal creep tests are shown on Figures 12 and 13. The continuous lines show the hyperbolic relation between log(strain) and log(time) which was used for the theoretical work.

4.3 Calculated stress redistribution

Figure 16 shows the radial temperature pattern and also the calculated stresses in the tube before, during and after stress redistribution. Figure 17 shows the time variation of axial stress, according to both time and strain hardening hypotheses. The small difference between the hypotheses as shown on Figure 18 arises from the relatively small stress changes involved, and the fact that some stresses are increasing while others are decreasing[14]. It has been shown elsewhere[15] that the differences are also small for turbine blade redistribution calculations, although in that case the stress changes can be much larger. Figure 17 also shows results calculated more simply by ignoring the radial constraints - that is by envisaging the tube as a set of separated concentric tubes each with its own uniform temperature and uniaxial stress but having the same total lengths. It is evident that ignoring the constraints causes an under-estimate of the thermal stresses and the time required for redistribution. The final distribution is unaffected because in this example, and in the case of turbine blades, the final distribution happens to be uniaxial.

Figure 18 shows the time variation of hoop and radial stresses and Figure 19 the directions (in the octahedral plane) of the effective stress and strain components. It is apparent that the strain direction lags behind the stress direction as a consequence of the incremental flow rule (Section 3.3.3) but they both approach the uniaxial condition.

4.4 Measured and calculated strain results

Figure 20 compares the theoretical predictions and measured values of axial strain. The upper line shows theoretical values of axial elongation according to the theory (strain and time hardening hypotheses being indistinguishable). The dashed line at the lower end depicts the results of a calculation for a cylinder without thermal stresses but having the same mean axial stress and mean radial temperature. The other continuous lines are the measured strains (transferred from Figures 10 and 11) for the tubular specimens. The lower strain level of the observed readings is associated with the direct electric heating method which seems to give consistently longer rupture times and, in part to the theoretical values used to describe the creep behaviour. Figure 12 shows the latter to give rather high creep strains in the strain range from about 1 to 10 per cent.

Examination of Figure 20 does show that application of creep data, obtained under conditions of constant stress and temperature, to a stress redistribution problem gives a strain behaviour which agrees reasonably well with that actually observed. Moreover the result of predicting the rupture life on the basis of the fully redistributed stress pattern agrees very well with the observed values. This conclusion is important because it implies that redistribution occurs as the result of very small creep strains and hence with little damage - thus confirming an assumption inherent in the present methods of calculating turbine blade lives.

5.0 Conclusions

Experimental (relevant to Nimonic alloy 105 at 970°C and 4 t.s.i.)

1. There is no significant difference between rupture times for specimens with and without modest initial thermal stresses provided that the mean stress and temperature levels are identical and do not vary with time.

2. There is a slight but consistent tendency for specimens heated directly by an electric current to last longer than those heated to the same temperature in a furnace. The life increase is equivalent to a temperature reduction of about 2°C.

3. A comparison of axial and diametral strains on the tube experiments with a temperature gradient indicates that some volume increase occurred during the first 100 hr and was particularly significant in the initial stages.

4. The shape of the strain/time curve, measured by the optical extensometer on directly heated specimens containing a radial temperature gradient, corresponded closely with that measured by conventional extensometers on furnace heated specimens containing no temperature gradient.

5. There seemed to be no significant difference between the rupture times for the two shapes and three sizes of test specimen when all were furnace tested using the same type of testing machine.

6. Metallurgical examination showed that the electrically heated specimens failed in a manner typical of creep at the applied stress and temperature levels.

7. A simple optical extensometer has been made and shown capable of resolving to about ±0·025 per cent on a gauge length of 0·625 in. without needing mechanical connections to the specimen.

Theoretical

1. An analytical solution has been derived for the stress distribution in a long thick cylinder containing an arbitrary distribution of non-elastic strains. The non-elastic strains may include any combination of thermal, creep and plastic strains, while the boundary conditions may include any combination of internal and external pressures and any axial mean stress.

2. The analysis has been incorporated into an Elliott 803 Autocode computer program. The program has been used, together with creep data derived from creep tests on the same batch of Nimonic alloy 105, to predict the behaviour of the tube during the process of stress redistribution arising from the initial thermal stress situation.

3. The results of the calculation show themselves relatively insensitive to the "hardening hypothesis" used because stress changes are relatively small and because some stresses increase as others decrease[14].

4. A simpler analysis ignoring radial and circumferential stresses (and therefore radial continuity of displacement) is shown to lead to an under-estimate of both the magnitude of the thermal stresses and the time required for them to redistribute. The simpler analysis does however give correct values for the redistributed stress pattern because in this particular case (no internal or external pressure) the radial and circumferential stresses disappear.

5. The predicted shape of strain/time curve corresponds except at extremely small strains and times with that of a uniformly stressed specimen having the same mean stress and temperature. Thus the theory and experiment both indicate an overall creep behaviour and rupture life consistent with mean stress/mean temperature conditions.

ACKNOWLEDGEMENTS

The author gratefully acknowledges the assistance given by Mr. J. E. Northwood and Mr. G. R. M. Jackson, who prepared the photomicrographs, and by the Staff of the Instrument Section who constructed the optical extensometer and carefully welded thermocouples at "impossible" positions.

REFERENCES

No.	Author(s)	Title, etc.
1	J. F. Barnes J. M. Clarke	The significance of creep in cooled gas turbine blades Conference on thermal loading and creep in structures and components (May 1964) Proc.I.Mech.E. p.43, Vol. 178, Part 3L
2	Henry Wiggin & Co. Ltd.	The Nimonic series of high temperature alloys
3	G. P. Tilly	Effects of varied loading paths on fatigue endurances. Part III - Some stress fatigue properties of H.46 at elevated temperatures A.R.C. Current Paper No. 788, 1964
4	S. Timoshenko	Theory of elasticity McGraw-Hill, 1934, p.366
5	A. E. Johnson J. Henderson V. Mathur	Creep under changing complex stress systems The Engineer, p.209, Vol. 206, 1958
6	A. Mendelson M. H. Hirschberg S. S. Manson	A general approach to the practical solution of creep problems Trans. A.S.M.E. Series D.J. Basic Eng. Vol. 5, No. 20, 1960
7	Y. N. Rabotnov	On the equation of state of creep Proc. Joint Int. Conference on Creep New York - London pp.2 to 117, 1963
8	A. Graham	The phenomenological method in rheology Research p.92, Vol. 6, 1953
9	A. Graham K. F. A. Walles	Relationships between long and short time properties in a commercial alloy Journal Iron and Steel Inst. p.105, Vol. 179, 1955
10	J. M. Clarke	A convenient representation of creep strain data for problems involving time-varying stresses and temperatures A.R.C. Current Paper No. 945, 1966
11	A. Phillips L. Kaechele	Combined stress tests in plasticity J.Appl.Mech. 23 (1956) 43

REFERENCES (cont'd)

No.	Author(s)	Title, etc.
12	J. Marin L. W. Hu	Biaxial plastic stress-strain relations of a mild steel for variable stress ratios Trans. A.S.M.E. 78 (1956) pp.499 to 509
13	J. C. Levy I. I. Barody	Poisson's ratio in creep using the strain-replica method Conference on thermal loading and creep in structures and components (May 1964) Proc.I.Mech.E. p.193, Vol. 178, Part 3L
14	J. M. Clarke	Conference on thermal loading and creep in structures and components Discussion at Session 4 Proc.I.Mech.E p.169, Vol. 178, Part 3L
15	J. M. Clarke	Unpublished work at N.G.T.E. 1964

TABLE I

Rupture times, reduction of area and test conditions

Note T_{25} = temperature below which 25 per cent of test duration was spent

T_{50} = temperature below which 50 per cent of test duration was spent

T_{75} = temperature below which 75 per cent of test duration was spent

T_{25}, T_{50}, T_{75} were derived from measurements by the thermocouple nearest to the rupture line

Test	Stress (t.s.i.)	T_{25} °C	T_{50} °C	T_{75} °C	Rupture time hr	% Reduction of area
A	4.0	970.0	970.2	970.7	515	18.4
B	4.0	970.6	971.6	972.7	464	18.5
C	4.0	968.5	969.4	970.0	485	18.4
D	4.0	967.1	967.3	967.5	508	17.4
E	3.96	966.5	967.5	968.3	553	17.0
F	4.0	969.0	969.4	969.8	415	16.5
G	7.0	964.7	964.9	965.0	33	29.1
H	7.0	964.5	964.6	964.8	31 < t < 32.5	(19.5)*
I	7.0	963.8	964.3	964.7	38	33.7
J	4.0	969.3	969.7	970.0	415	21.6
K	4.0	969.3	969.8	970.0	374	20.9
L	4.0	969.8	969.9	970.1	408	19.5
M	7.0	964.5	964.6	964.8	34	31.7
N	4.0	968.4	969.6	970.0	396	13.5

*This test was terminated by a power failure after 31 hr but the strain record showed that rupture would have occurred before 32.5 hr. The percentage reduction of area was for a low temperature fracture caused by the specimen's contraction while cooling.

TABLE II

Derived creep properties for Nimonic 105 fully heat treated. Cast AE 148

(For explanation of symbols see Reference 10)

Symbol	Value						Units
θ	27.8						Degrees of arc
ϕ	75.0						Degrees of arc
A	0.863						Natural log cycles
B	-6.430						Natural log cycles
C	0						Natural log cycles/(ton/in^2)
at	900°C	920°C	940°C	960°C	980°C	1000°C	
D	10.45	9.81	9.29	8.81	8.39	7.97	Natural log cycles
E	-0.62	-0.680	-0.758	-0.850	-0.960	-1.10	Natural log cycles/(ton/in^2)

APPENDIX I

Notation

a, b	arbitrary constants
c	non-elastic strain
E	Young's modulus
e	total strain (elastic + thermal + creep)
F(r), G(r), H(r)	functions of radius
P	pressure
p, q	arbitrary constants
r	radius
R, S	constants of integration
s	mean axial stress
T	temperature
t	time
u	radial displacement
v, w	stress and temperature sensitivities of strain rate
x, y	co-ordinates of $\ln(\varepsilon/\lambda)$ versus $\ln(t/\tau)$ curve
α	temperature coefficient of linear expansion
ε	creep strain
$\bar{\varepsilon}$	effective creep strain
λ	a reference strain
υ	Poisson's ratio
σ	stress
$\bar{\sigma}$	effective stress
τ	a reference time

Notation (cont'd)

Subscripts

1 , 2	before and after a time increment
1 , 2 , 3	axial radial and hoop directions
i, o	inside and outside surfaces
s	strain hardening hypothesis
t	time hardening hypothesis
max	maximum
mean	area mean

APPENDIX II

Calculation of stresses in a long thick-walled tube with arbitrary mean axial stress, inside and outside pressures and radial distribution of non-elastic strains

Hooke's law in the presence of non-elastic strains may be written:

$$\left.\begin{aligned} e_1 &= \frac{1}{E}\sigma_1 - \frac{\nu}{E}(\sigma_2 + \sigma_3) + c_1 \\ e_2 &= \frac{1}{E}\sigma_2 - \frac{\nu}{E}(\sigma_1 + \sigma_3) + c_2 \\ e_3 &= \frac{1}{E}\sigma_3 - \frac{\nu}{E}(\sigma_2 + \sigma_1) + c_3 \end{aligned}\right\} \quad \ldots\ldots(II.1)$$

Elimination of σ_1 from the above and some re-arrangement gives:

$$\sigma_2 = \frac{E\nu}{(1-2\nu)(1+\nu)}\left((e_1 - c_1) + (e_2 - c_2) + (e_3 - c_3)\right) + \frac{E}{1+\nu}\left((e_1 - c_2)\right) \quad \ldots\ldots(II.2)$$

$$\sigma_2 - \sigma_3 = -\frac{E}{1+\nu}\left((e_2 - e_3) - (c_2 - c_3)\right) \quad \ldots\ldots(II.3)$$

The radial equilibrium condition in the absence of body forces is:

$$\frac{d\sigma_2}{dr} + \frac{\sigma_2 - \sigma_3}{r} = 0 \quad \ldots\ldots(II.4)$$

and the compatability condition under the assumed axisymmetric and longitudinally uniform conditions is:

$$\left.\begin{aligned} e_1 &= \text{constant} \\ e_2 &= \frac{du}{dr} \\ e_3 &= \frac{u}{r} \end{aligned}\right\} \quad \ldots\ldots(II.5)$$

Substitution from (II.5) into (II.2) and (II.3) and then from (II.2) and (II.3) into (II.4) leads to the following second order non-homogeneous ordinary differential equation for the displacement:

$$\frac{d}{dr}\left(\frac{du}{dr} + \frac{u}{r}\right) = F(r) \qquad \ldots\ldots(II.6)$$

where $$F(r) = \frac{\upsilon}{1-\upsilon}\frac{d}{dr}(c_1 + c_2 + c_3) + \frac{1-2\upsilon}{1-\upsilon}\left(\frac{dc_2}{dr} + \frac{c_2 - c_3}{r}\right)$$

$\ldots\ldots(II.7)$

Two integrations of (II.6) lead to the form of the solution for displacement:

$$u = Rr + S\frac{r_i^2}{r} + \frac{1}{r}\int_{r_i}^{r} r \int_{r_i}^{r} F(r)\, dr\, dr \qquad \ldots\ldots(II.8)$$

and for convenience the notation

$$G(r) = \int_{r_i}^{r} F(r)\, dr$$

$$H(r) = \frac{1}{r^2}\int_{r_i}^{r} r\, G(r)\, dr$$

is introduced so that (II.8) can be written

$$u = Rr + Sr_i^2\frac{1}{r} + r\,H(r) \qquad \ldots\ldots(II.9)$$

The problem is therefore reduced to finding the constants R, S and e_1, such that the following boundary conditions apply

$$\left.\begin{array}{lll} \text{(i)} & \sigma_{zi} = -P_i & \text{the inside pressure} \\ \text{(ii)} & \sigma_{zo} = -P_o & \text{the outside pressure} \\ \text{(iii)} & 2\int_{r_i}^{r_o} \sigma_z r\, dr/(r_o^2 - r_i^2) = s & \text{the mean axial stress} \end{array}\right\} \qquad \ldots\ldots(II.10)$$

Substitution from (II.5) into (II.2) expresses σ_z in terms of u and its derivative so that Equation (II.8) is then available to express σ_z in terms of the constants R, S and e_1.

$$\sigma_2 = \frac{E}{(1-2\nu)(1+\nu)}(R + \nu e_1) - \frac{E}{(1+\nu)}\left(S\frac{r_i^2}{r^2} + H(r)\right)$$

$$+ \frac{E(1-\nu)}{(1-2\nu)(1+\nu)}\left(G(r) - c_2\right) - \frac{E\nu}{(1-2\nu)(1+\nu)}(c_1 + c_3)$$

....(II.11)

Substitution for $\sigma_2 = -P_i$ at $r = r_i$ and $\sigma_2 = -P_o$ at $r = r_o$ leads to values for $(R + \nu e_1)$ and S

$$S = \frac{r_o^2}{r_o^2 - r_i^2}\left\{\frac{1+\nu}{E}(P_i - P_o) - \frac{1-\nu}{1-2\nu}G(r_o) + H(r_o)\right.$$

$$\left. + \frac{\nu}{1-2\nu}\left((c_{1o} - c_{1i}) + (c_{3o} - c_{3i})\right) + \frac{1-\nu}{1-2\nu}(c_{2o} - c_{2i})\right\}$$

....(II.12)

$$R + \nu e_1 = S(1-2\nu) - \frac{(1-2\nu)(1+\nu)}{E}P_i + (1-\nu)c_{2i} + \nu(c_{1i} + c_{3i})$$

....(II.13)

The last two equations permit σ_2 to be found using (II.11) then σ_3 can be found from:

$$\sigma_2 - \sigma_3 = \frac{E}{1+\nu}\left(2S\frac{r_i^2}{r^2} + 2H(r) - G(r) + (c_2 - c_3)\right) \quad ....(II.14)$$

The radial and hoop stresses have now been determined but the third boundary condition has not been introduced. This can now be done by integrating the first equation in II.1.

$$\text{Hence} \quad e_1 = \frac{2}{r_o^2 - r_i^2}\left\{\frac{1}{g}\int_{r_i}^{r_o} r\sigma_1\, dr - \frac{v}{g}\int_{r_i}^{r_o}(\sigma_2 + \sigma_3)rdr + \int_{r_i}^{r_o} c_1 rdr\right\}$$

$$\text{i.e.,} \quad e_1 = \frac{s}{g} - \frac{2}{r_o^2 - r_i^2}\left\{\frac{v}{g}\int_{r_i}^{r_o}(\sigma_2 + \sigma_3)rdr - \int_{r_i}^{r_o} c_1 rdr\right\} \quad \ldots\ldots(II.15)$$

Sufficient information is now available to calculate σ_1 from the first equation in II.1, and the displacement function u from the solution II.8.

APPENDIX III

Some conditions required for the establishment of a steady state stress distribution in a uniaxial axisymmetric situation

The analysis which follows illustrates a number of properties of the 'fully redistributed' or 'steady state' stress pattern which is generally achieved after stress redistribution calculations.

It is shown that if the log(creep strain)/log(time) curves are of the same shape and simply displaced for different stresses and temperatures then the existence of a general steady state requires that the shape involved is a member of a family of curves containing three arbitrary constants and including as a sub-set all straight lines. A method is shown for calculating directly the redistributed solution.

It is assumed that the creep strain/time results of ordinary creep tests over a range of stresses and temperatures can be represented by a formula of the form:

$$\ln\left(\frac{\varepsilon}{\lambda}\right) = f_1\left(\ln\left(\frac{t}{\tau}\right)\right) \qquad \ldots.(III.1)$$

or for convenience:

$$y = f_1(x) \qquad \ldots.(III.2)$$

where the function f_1 does not depend on stress or temperature but λ and τ can each depend on both stress and temperature. The function f_1 is for the moment arbitrary and so are λ and τ which are the strain and time values for which y and x respectively are zero. A hyperbolic relation between x and y is used in Reference 10 and also in the theoretical work described in this Report.

It can be shown that the corresponding expression for strain rate is:

$$\frac{d\varepsilon}{dt} = \frac{dy}{dx} \cdot \exp(y - x) \cdot \frac{\lambda}{\tau} \qquad \ldots.(III.3)$$

or

$$\frac{d\varepsilon}{dt} = f_2(x) \cdot \frac{\lambda}{\tau} \qquad \ldots.(III.4)$$

where

$$f_2(x) = \frac{dy}{dx} \cdot \exp(y - x) \qquad \ldots.(III.5)$$

Now in a uniaxial axisymmetric stress situation in which neither the stress nor temperature are changing with time the creep strain rate (say $\dot{\varepsilon}_1$) must be the same at all positions, so that

$$f_2(x) = \dot{\varepsilon}_1 \tau/\lambda \qquad \ldots.(III.6)$$

where in general τ/λ and x will be different at different positions.

Some time later although τ/λ remains constant (because stresses and temperatures are constant) the strain rates (say $\dot{\varepsilon}_2$) common to all positions might be different, so that

$$f_2(x + \Delta x) = \dot{\varepsilon}_2 \tau/\lambda \qquad \ldots.(III.7)$$

Now
$$\Delta x = \ln\left(1 + \frac{\Delta t}{t}\right) \qquad \ldots.(III.8)$$

which is independent of x and is the same at all points hence

$$\frac{f_2(x + \Delta x)}{f_2(x)} = \frac{\dot{\varepsilon}_2}{\dot{\varepsilon}_1} \text{ for all } x, \qquad \ldots.(III.9)$$

i.e., the proportional change in f_2 with x does not depend on the instantaneous value of f_2. The most general function with this property is the exponential function which may be written:

$$f_2(x) = \exp(ax + b) \text{ where a, b are constants}$$

$$\ldots.(III.10)$$

or equivalently, and more conveniently in this case:

$$f_2(x) = p \exp\left((p - 1)\, x + q\right) \qquad \ldots.(III.11)$$

where p, q are constants. Comparison with (III.5) yields the differential equation

$$\exp(y) \cdot \frac{dy}{dx} = p \exp(px + q) \qquad \ldots.(III.12)$$

Integration of this equation gives:

$$y = \ln\left(\exp(px + q) + \exp(y_{-\infty}) \right) \qquad \ldots.(III.13)$$

where $y_{-\infty}$ is the value of y when $x = -\infty$.

An important special case of (III.13) is the straight line

$$y = px + q \qquad \ldots.(III.14)$$

which corresponds to a strain/time relation of the form

$$\varepsilon \propto t^p \qquad \ldots.(III.15)$$

and assumes zero creep strain at zero time.

Substitution from (III.11) into (III.4) gives

$$\frac{d\varepsilon}{dt} = p \exp\left((p - 1) x + q \right) \cdot \frac{\lambda}{\tau} \qquad \ldots.(III.16)$$

i.e., $$\frac{d\varepsilon}{dt} = p \exp(q) \cdot t^{p-1} \cdot \frac{\lambda}{\tau^p} \qquad \ldots.(III.17)$$

In the general case when both λ and τ vary with stress and temperature the steady state stress pattern must therefore satisfy (because the other term in (III.17) is the same for all elements):

$$\frac{\lambda}{\tau^p} = \text{constant} \qquad \ldots.(III.18)$$

and the constant can be obtained from the requirement that the integrated stress be equal to the applied load. The solution therefore depends on p unless λ is constant.

Simple example

Assuming the following variations of λ and τ with stress and temperature:

$$\left.\begin{aligned} \lambda &= \text{constant} \\ \tau &= \tau' \exp\Big(v(\sigma - \sigma') + w(T - T')\Big) \end{aligned}\right\} \qquad \ldots.(III.19)$$

Here τ', σ', T' are typical constant values for the time scale, stress and temperature of the problem while v and w represent sensitivities of τ to departures from σ' and T'.

Then for constant λ/τ^p as required by (III.18) for a steady state solution

$$\tau = \text{constant} \qquad \ldots.(III.20)$$

and from (III.19)

$$v(\sigma - \sigma') + w(T - T') = \text{constant} = K \qquad \ldots.(III.21)$$

Integrating with respect to area gives:

$$v \int \sigma dA + w \int T dA = (K + v\sigma' + wT') \int dA \qquad \ldots.(III.22)$$

i.e.,

$$v(\sigma_m - \sigma') + w(T_m - T') = K \qquad \ldots.(III.23)$$

where σ_m and T_m are area mean values of stress and temperature.

From (III.23) and (III.19) it follows that the effective time scale factor τ for the non-uniform system corresponds to that obtainable from a uniform stress situation at the same mean stress and temperature.

It should be emphasised that the relatively simple expressions (III.19) which led to this conclusion only apply for rather limited departures of stress and temperature from the σ', T' values. Nevertheless the analysis serves to illustrate that the strain accumulation after redistribution corresponds roughly with mean stress/mean temperature conditions and the solution of (III.18) with more accurate forms of (III.19) gives a useful technique for the direct calculation of steady state stress patterns from applied temperature patterns.

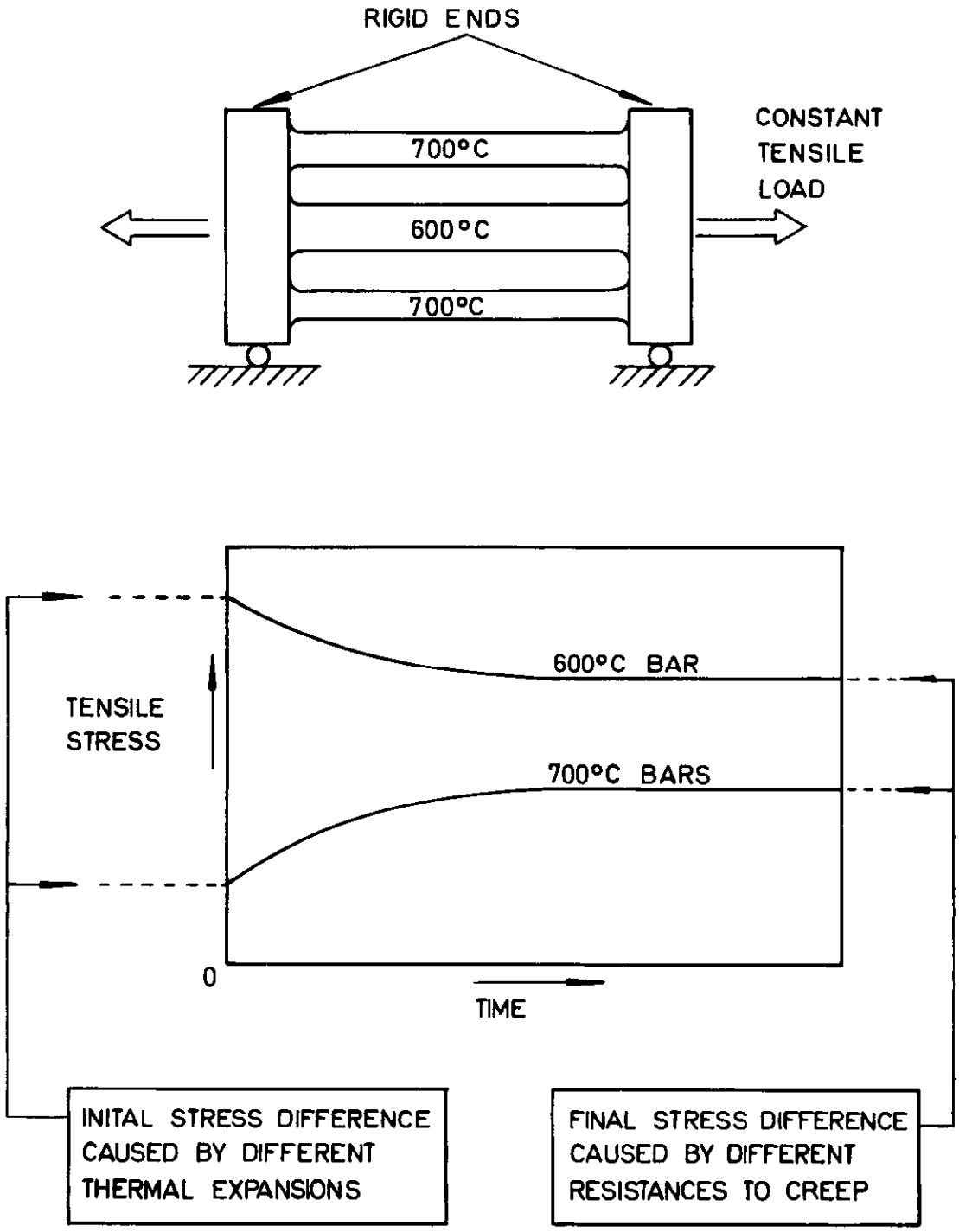

FIG 1 STRESS REDISTRIBUTION IN A SIMPLE TENSILE SYSTEM

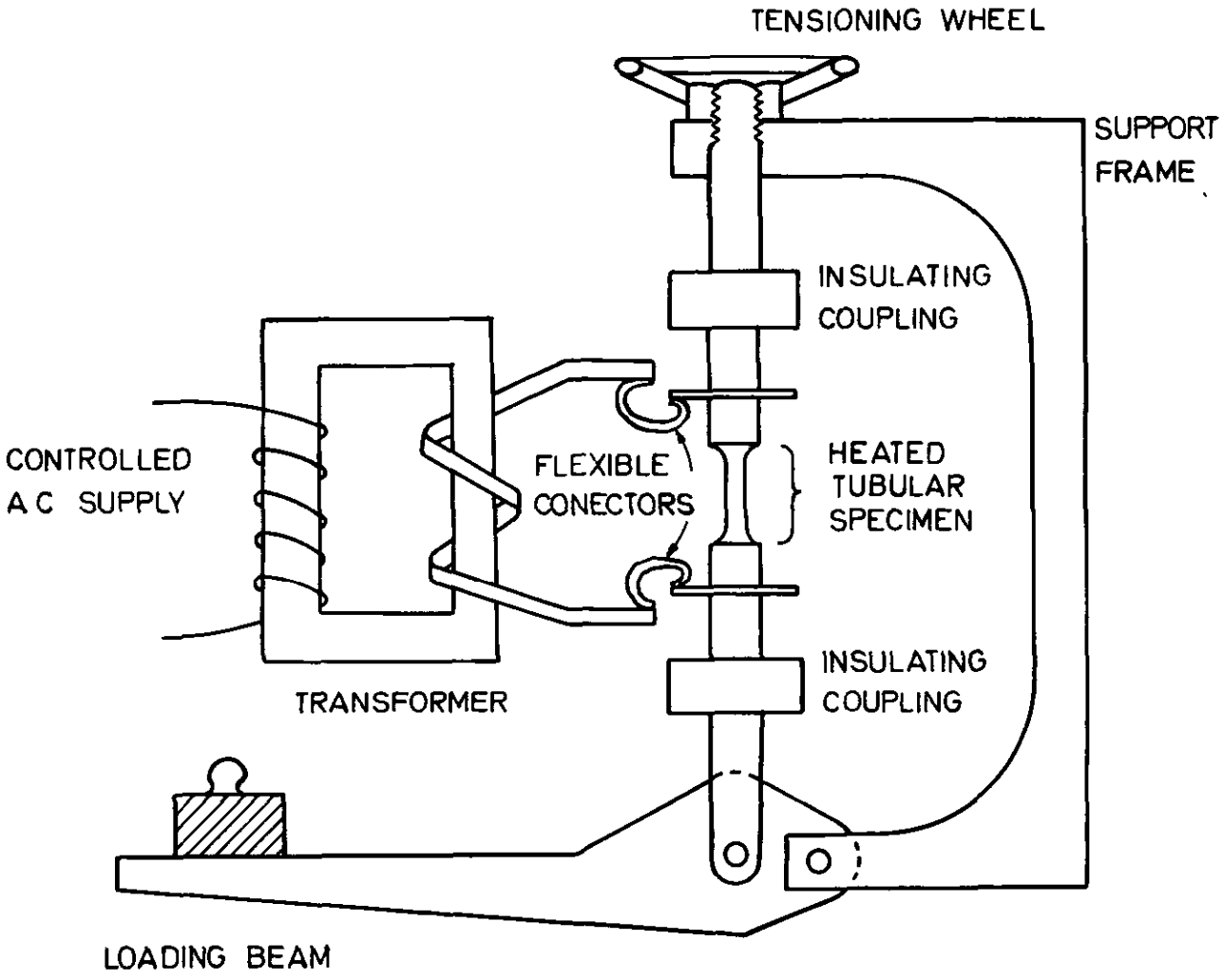

FIG 2 SCHEMATIC ARRANGEMENT OF APPARATUS

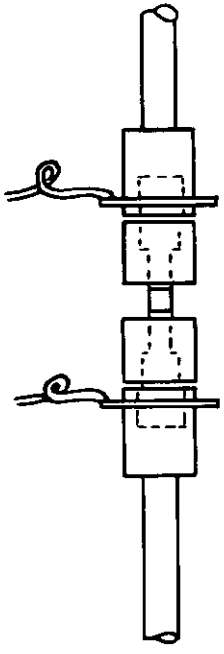	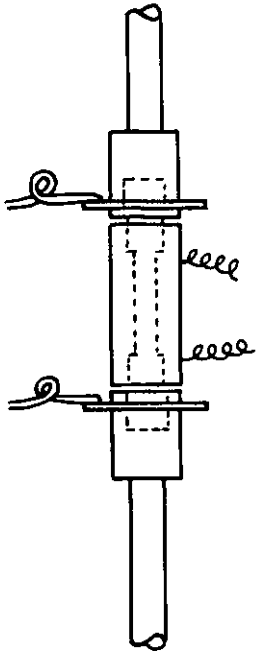	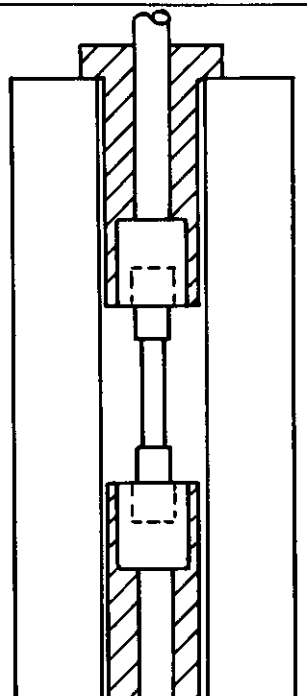	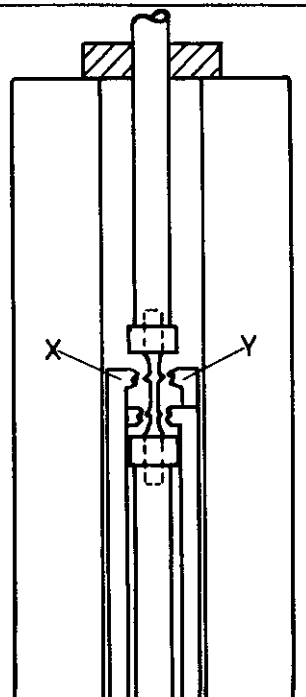	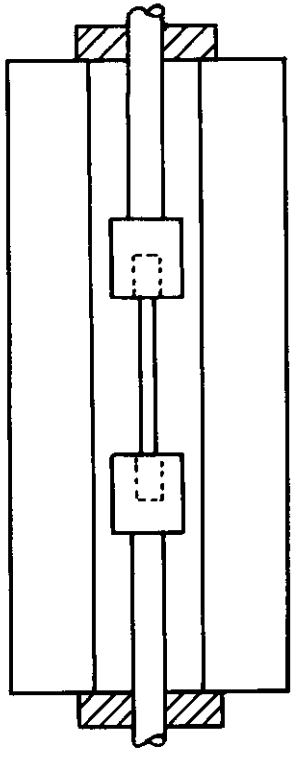
TYPE 1	TYPE 2	TYPE 3	TYPE 4	TYPE 5
TUBE SPECIMEN DIRECT ELECTRIC HEATING CENTRE PORTION FREE TO RADIATE RADIAL TEMP GRADIENT INSIDE TEMP 970°C	TUBE SPECIMEN DIRECT ELECTRIC HEATING CENTRE PORTION ALSO HEATED BY AUXILIARY ELEMENT NO RADIAL TEMP GRADIENT SAME MEAN TEMP AS TYPE 1	TUBE SPECIMEN FURNACE HEATED NO RADIAL TEMP GRADIENT. TEMP 970°C	SOLID CYLINDRICAL SPECIMEN FURNACE HEATED SOME TESTED AT 970°C 4 TON/IN^2 OTHERS AT 965°C 7 TON/IN^2 EXTENSOMETERS (X,Y) ATTACHED	SOLID CYLINDRICAL SPECIMEN. FURNACE HEATED SOME TESTED AT 970°C 4 TON/IN^2 OTHERS AT 965°C 7 TON/IN^2
TESTS A,B,C,	TESTS D, E,	TEST F,	TESTS G,H,I,J,K,L,	TESTS M,N,

FIG 3 EXPERIMENTAL ARRANGEMENTS

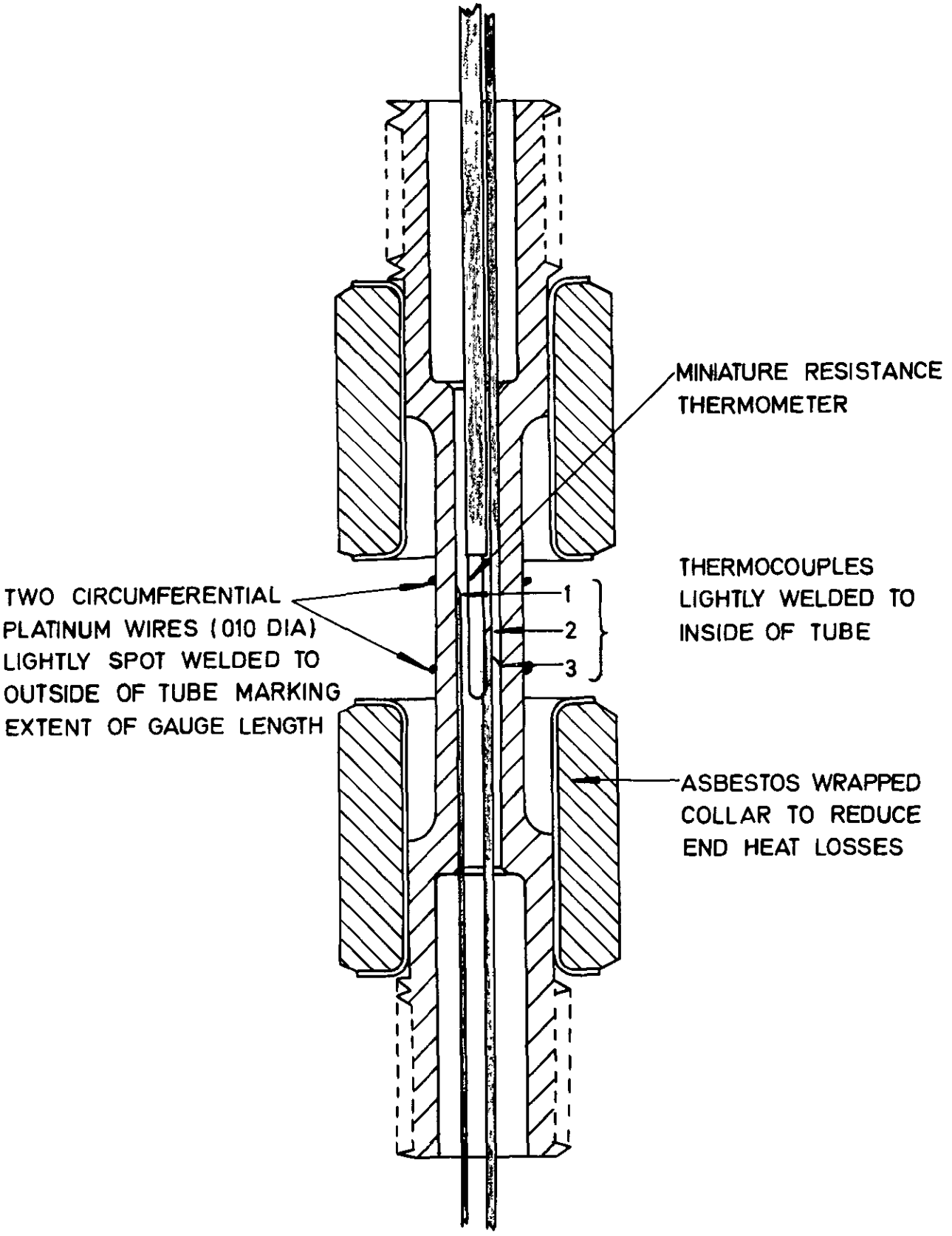

FIG 4 ARRANGEMENT NO 1 SHOWING INSTRUMENTATION

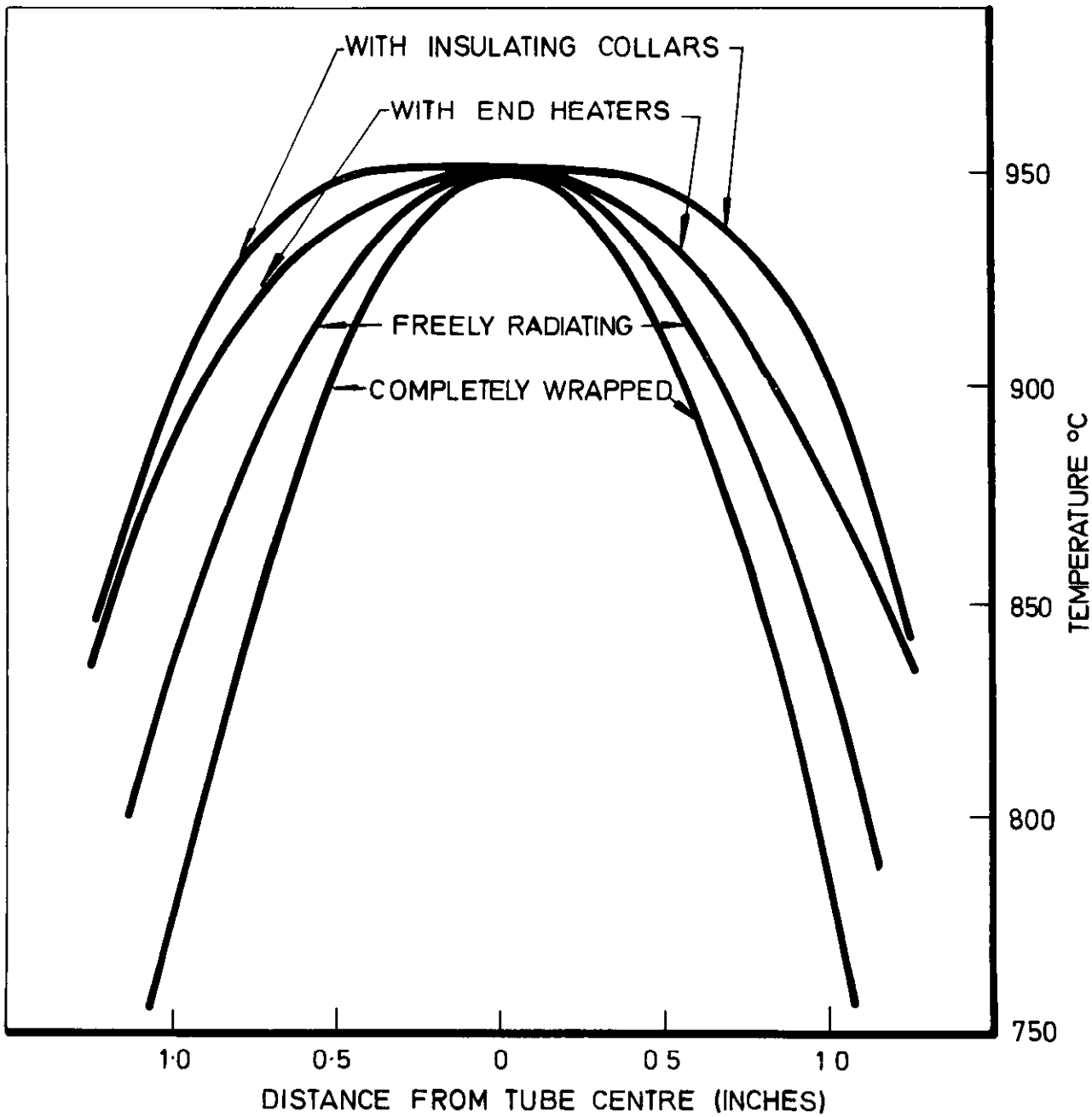

FIG 5 LONGITUDINAL TEMPERATURE PROFILES

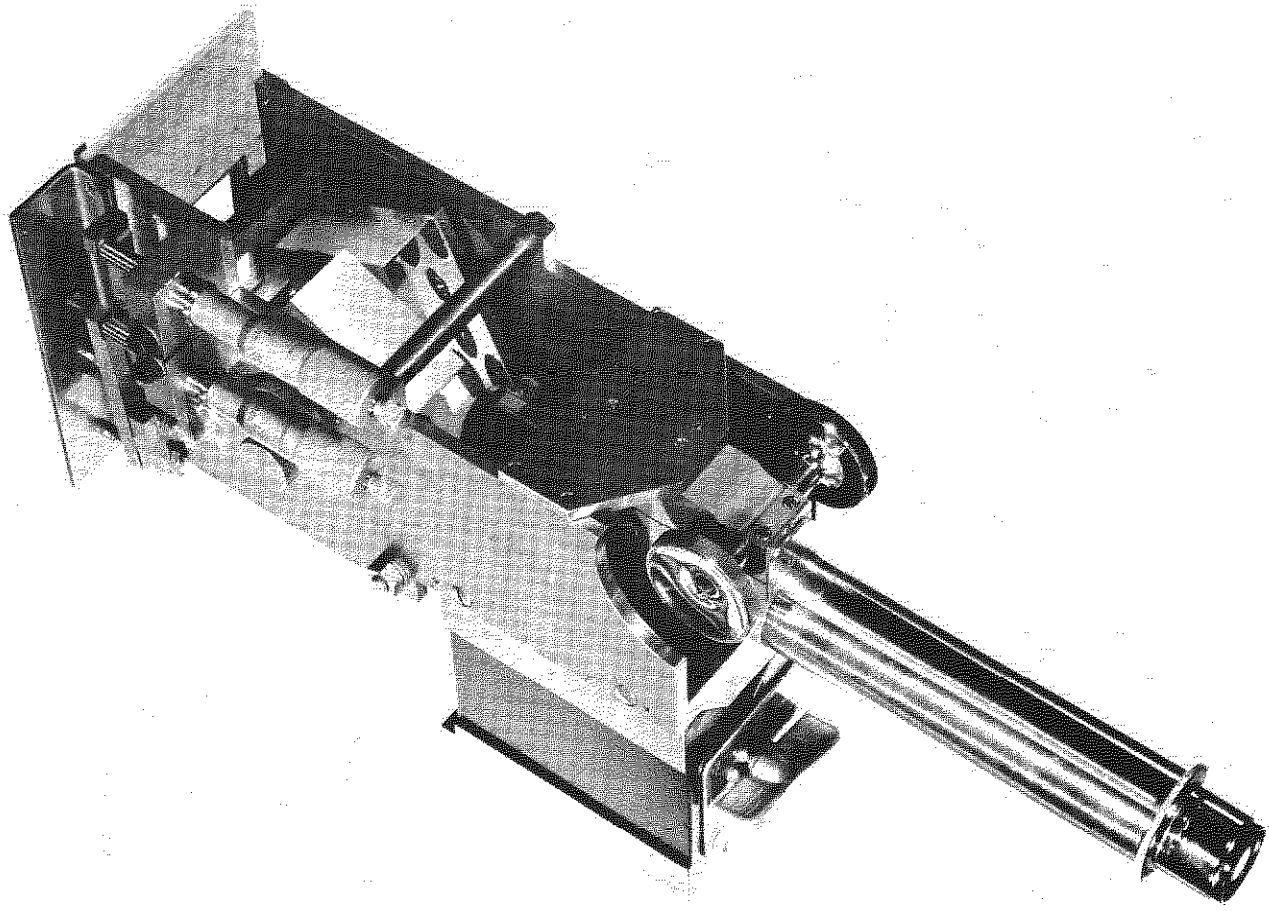

FIG 6 OPTICAL EXTENSOMETER

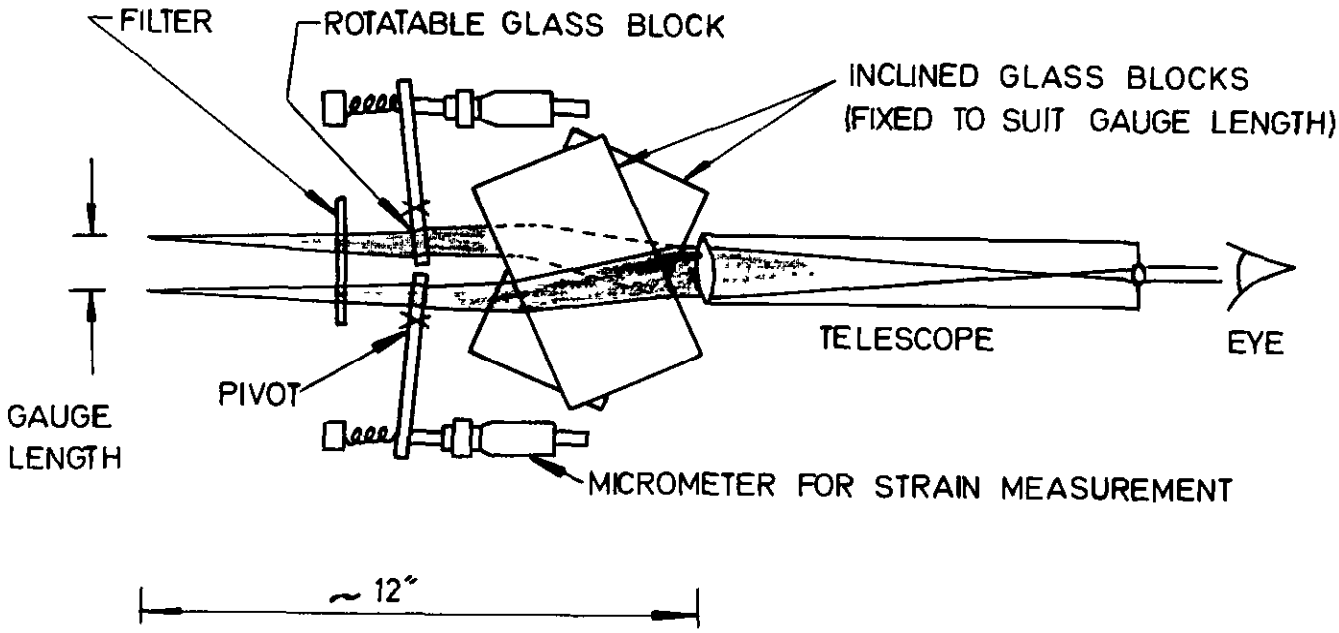

FIG 7 SCHEMATIC ARRANGEMENT SHOWING PRINCIPLE OF OPTICAL EXTENSOMETER

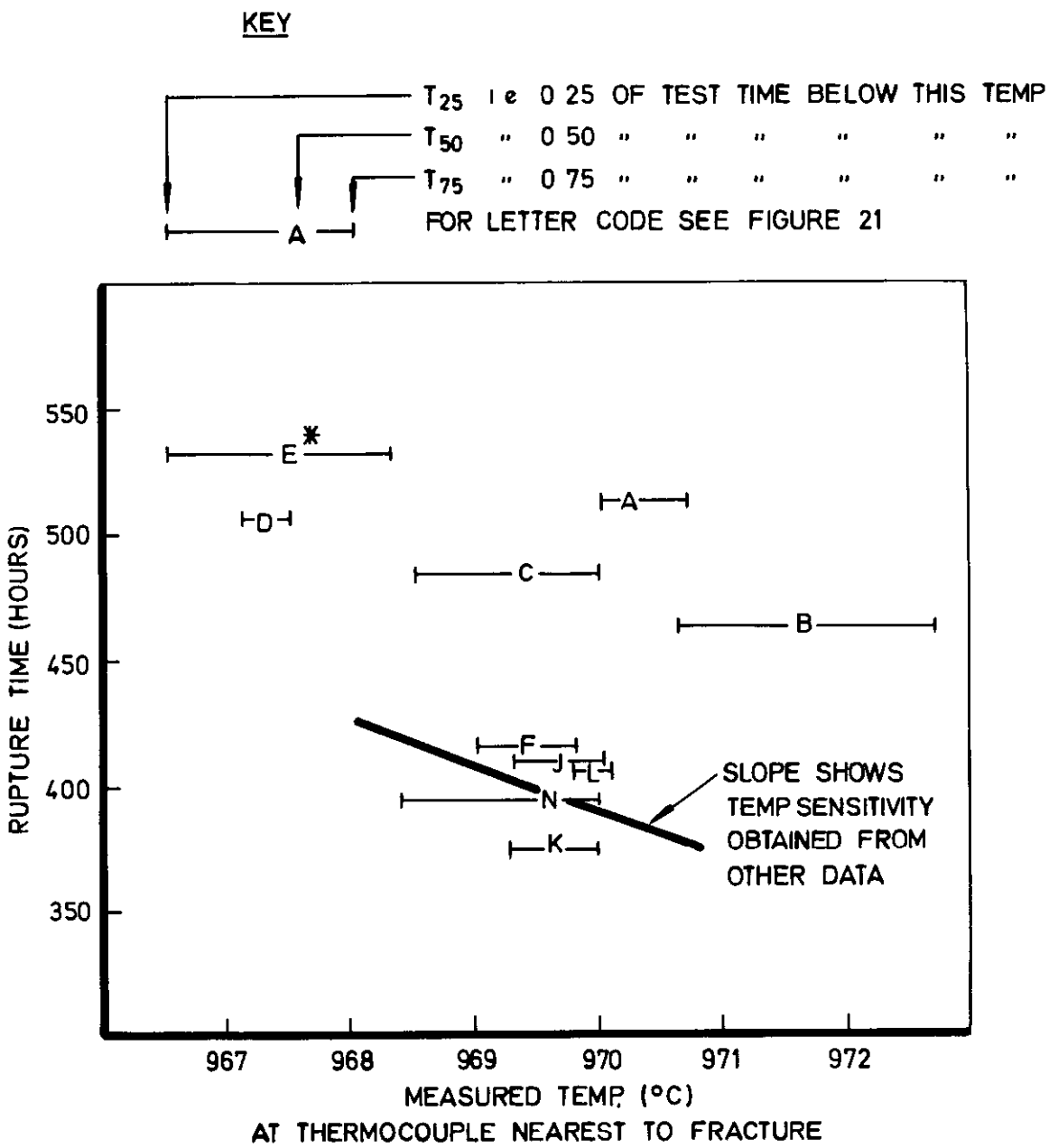

* RUPTURE TIME CORRECTED TO 4 TON/IN^2 FROM 3·96 TON/IN^2

FIG 8 RUPTURE TIMES FOR SPECIMENS STRESSED TO 4TON/IN^2

KEY AS FOR FIG 8

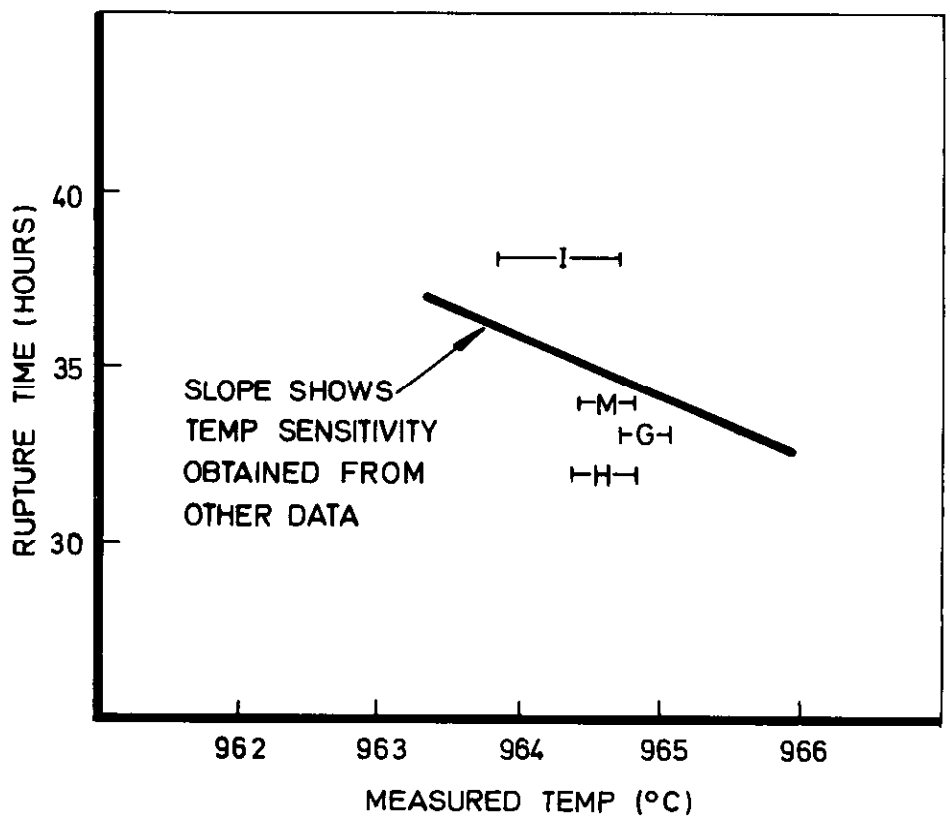

FIG 9 RUPTURE TIMES FOR SPECIMENS STRESSED TO 7 TON/IN^2

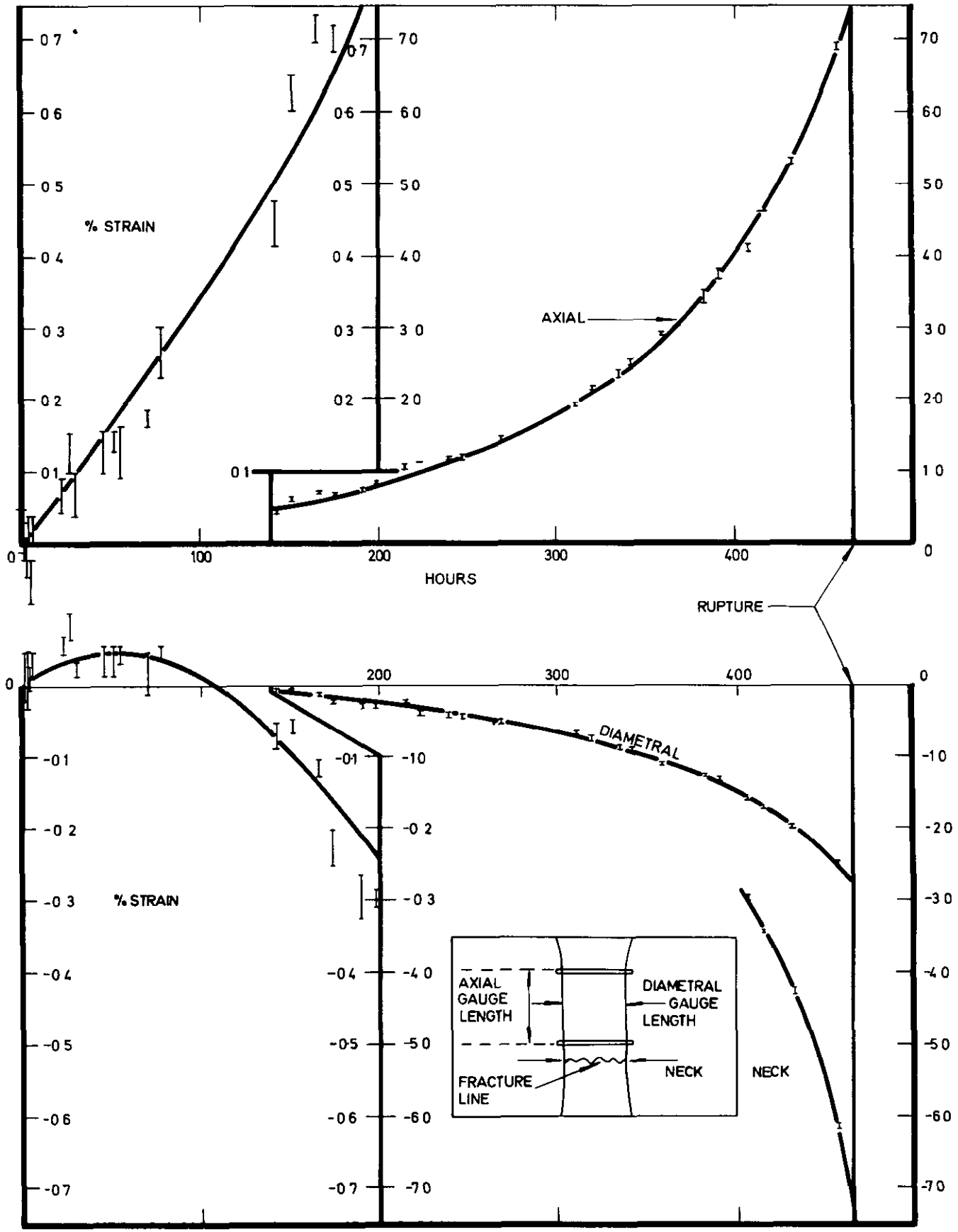

FIG 10 OPTICAL EXTENSOMETER STRAIN RESULTS - SPECIMEN B

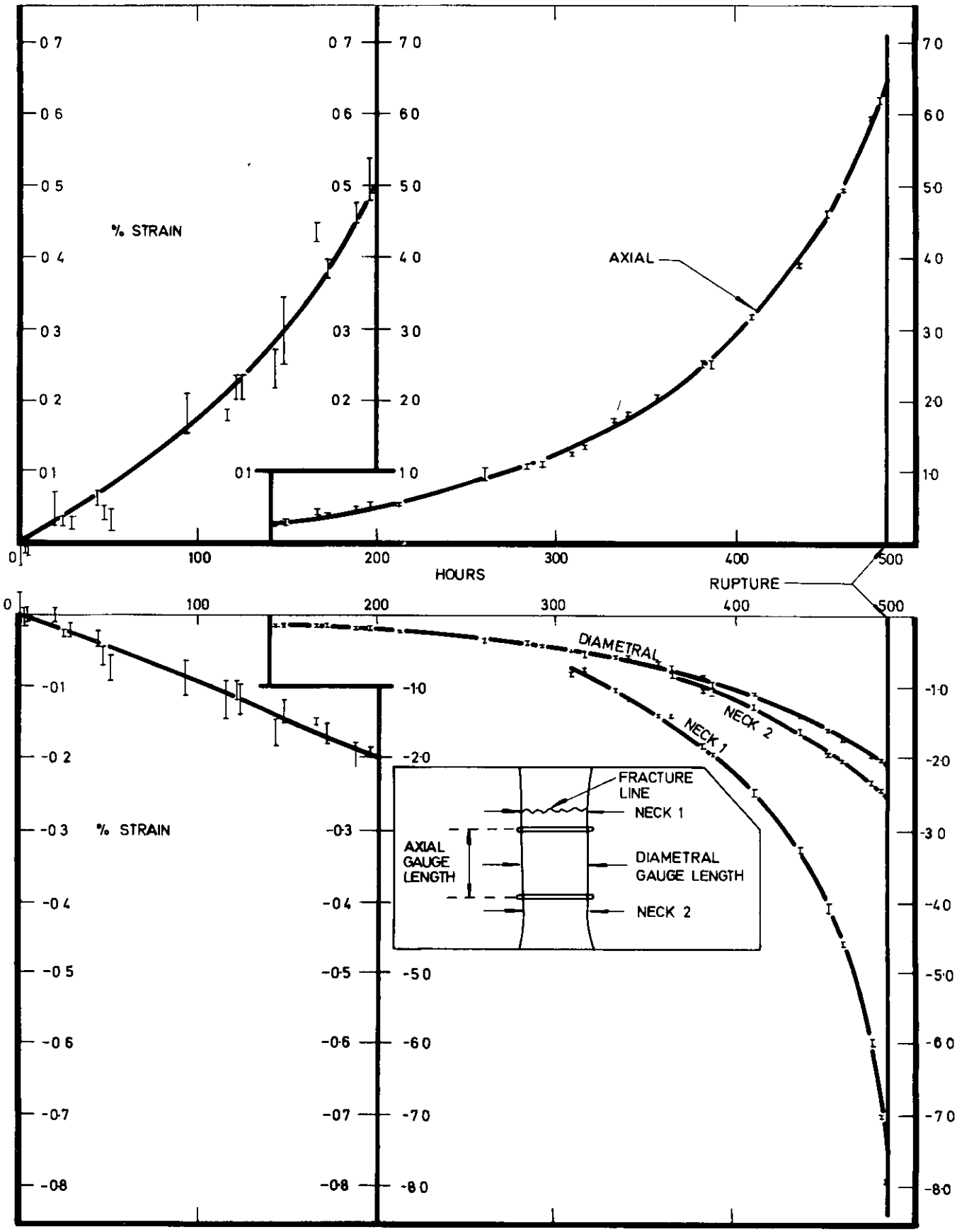

FIG 11 OPTICAL EXTENSOMETER STRAIN RESULTS - SPECIMEN C

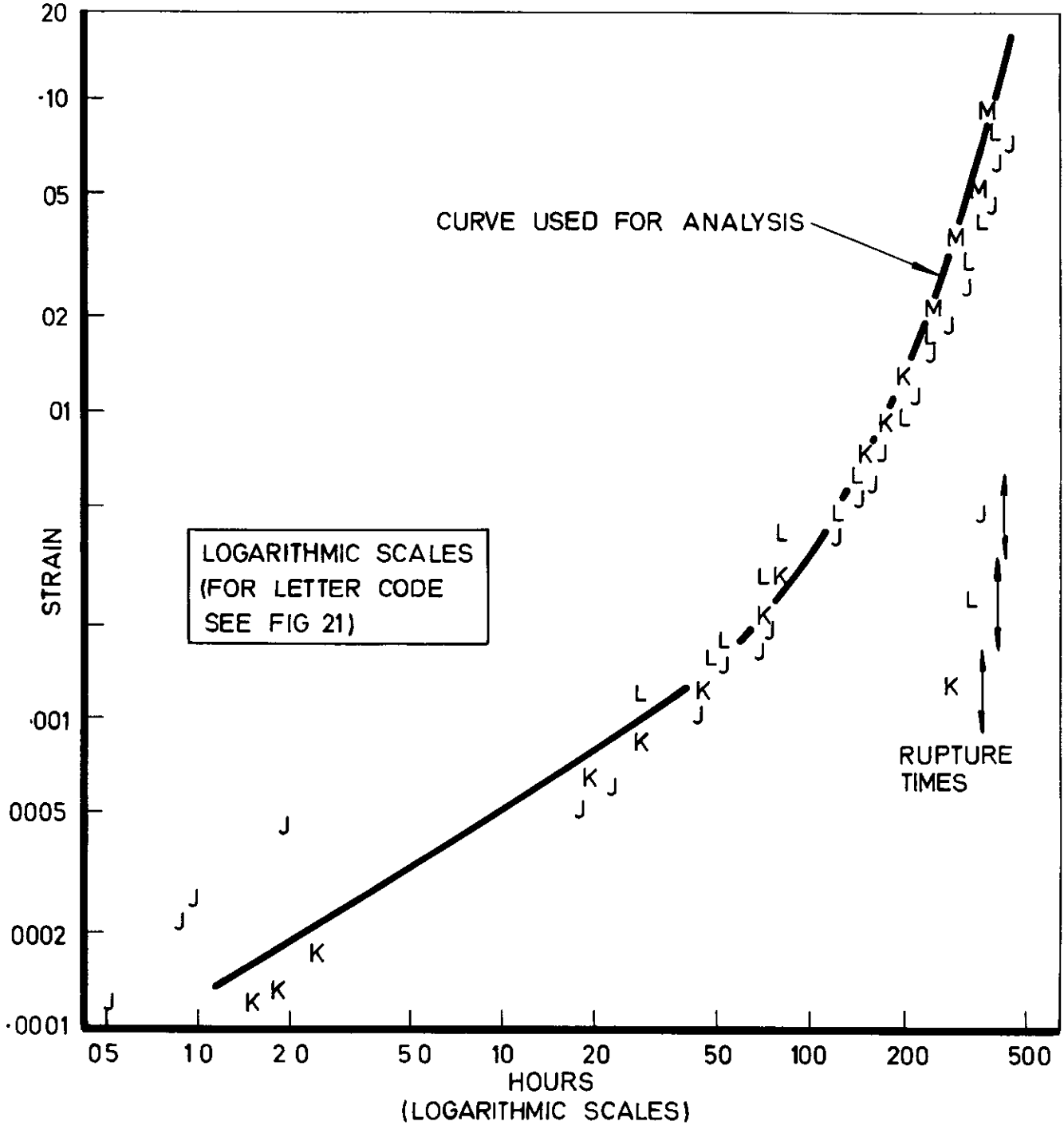

FIG 12 STRAIN RECORDS FOR TESTS AT 970°C, 4 TON/IN^2

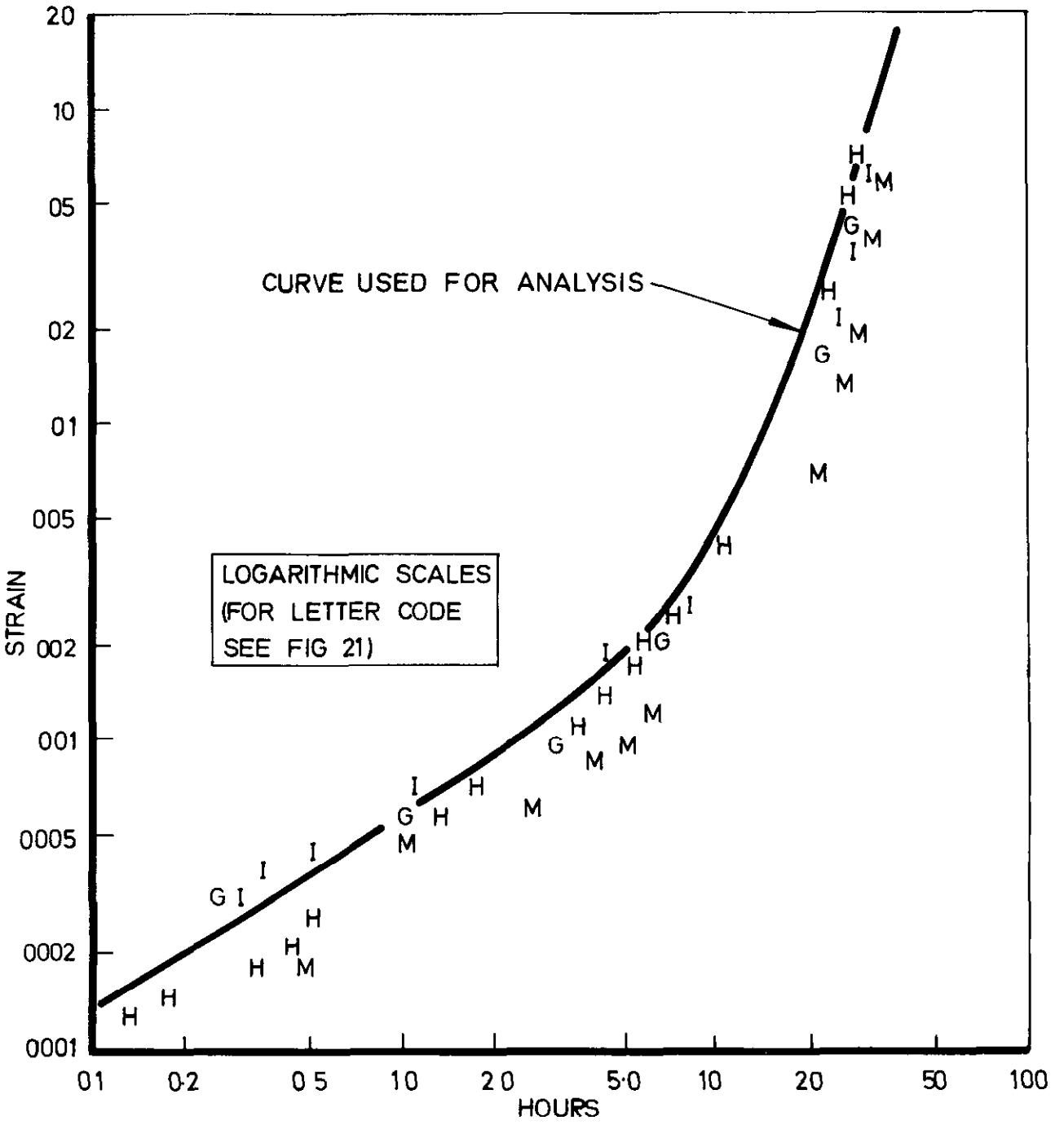

FIG 13 STRAIN RECORDS FOR TESTS AT 965°C, 7-TON/IN^2

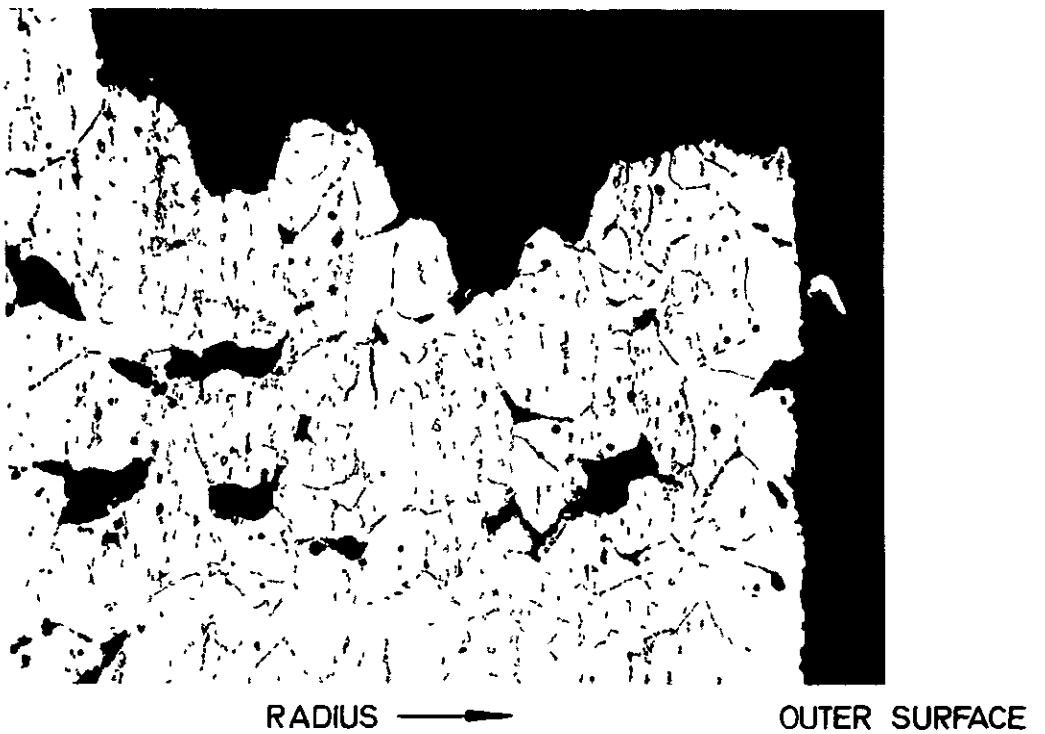

FIG 14 RADIAL SECTION THROUGH SPECIMEN C SHOWING FRACTURE SURFACE (X 100)

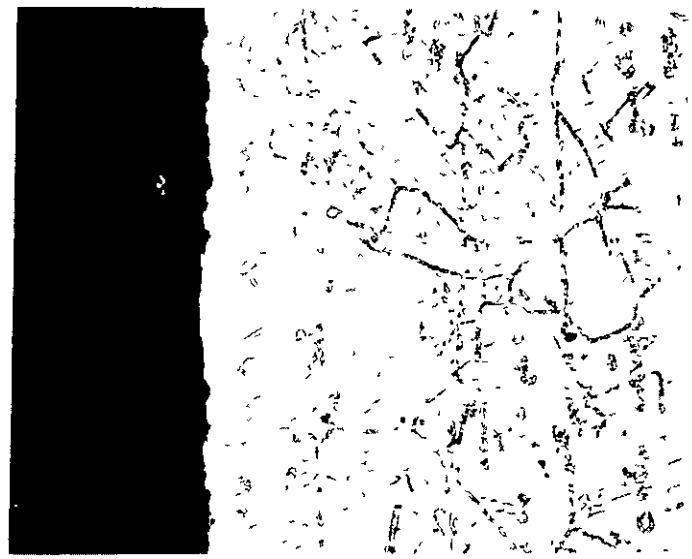

INSIDE SURFACE (X 200)

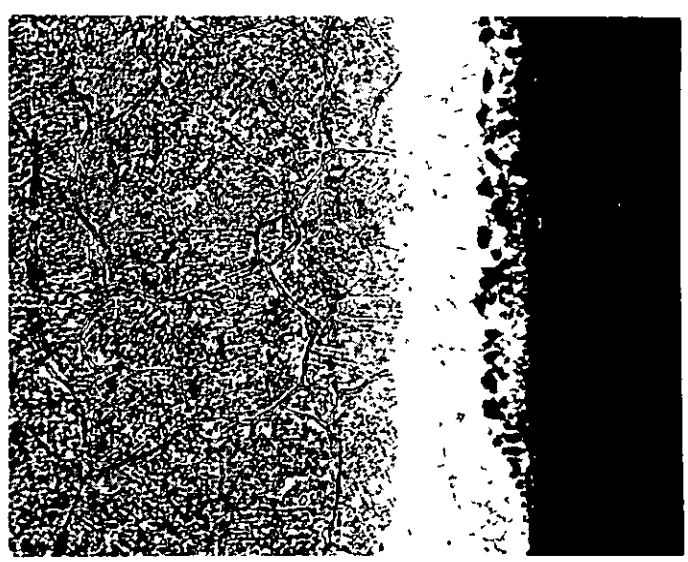

OUTSIDE SURFACE (X 200)

FIG 15 RADIAL SECTIONS THROUGH SPECIMEN C SHOWING OXIDATION AT INSIDE AND OUTSIDE SURFACES (X 200)

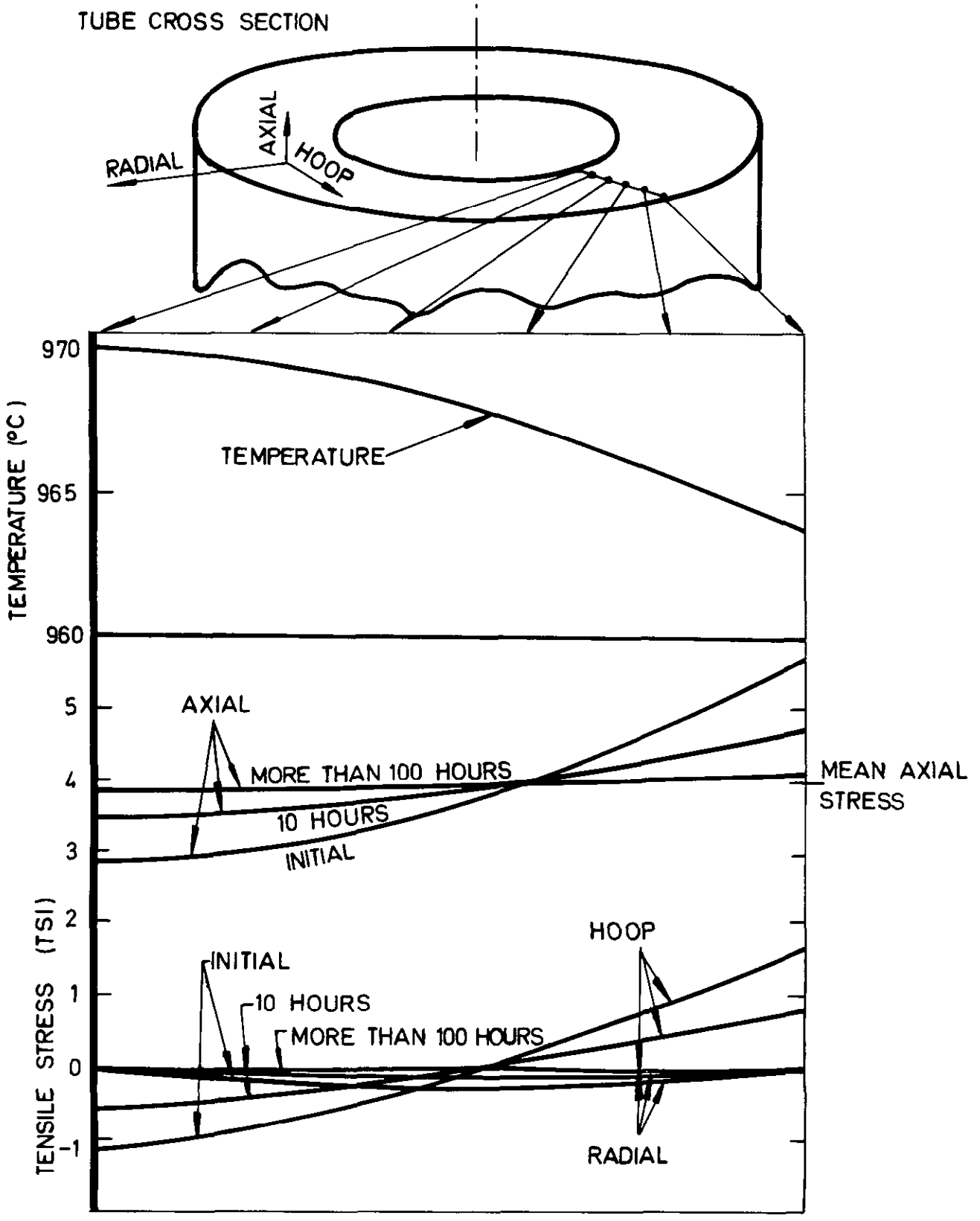

FIG 16 CALCULATED TEMPERATURE AND STRESS PROFILES BEFORE DURING AND AFTER REDISTRIBUTION

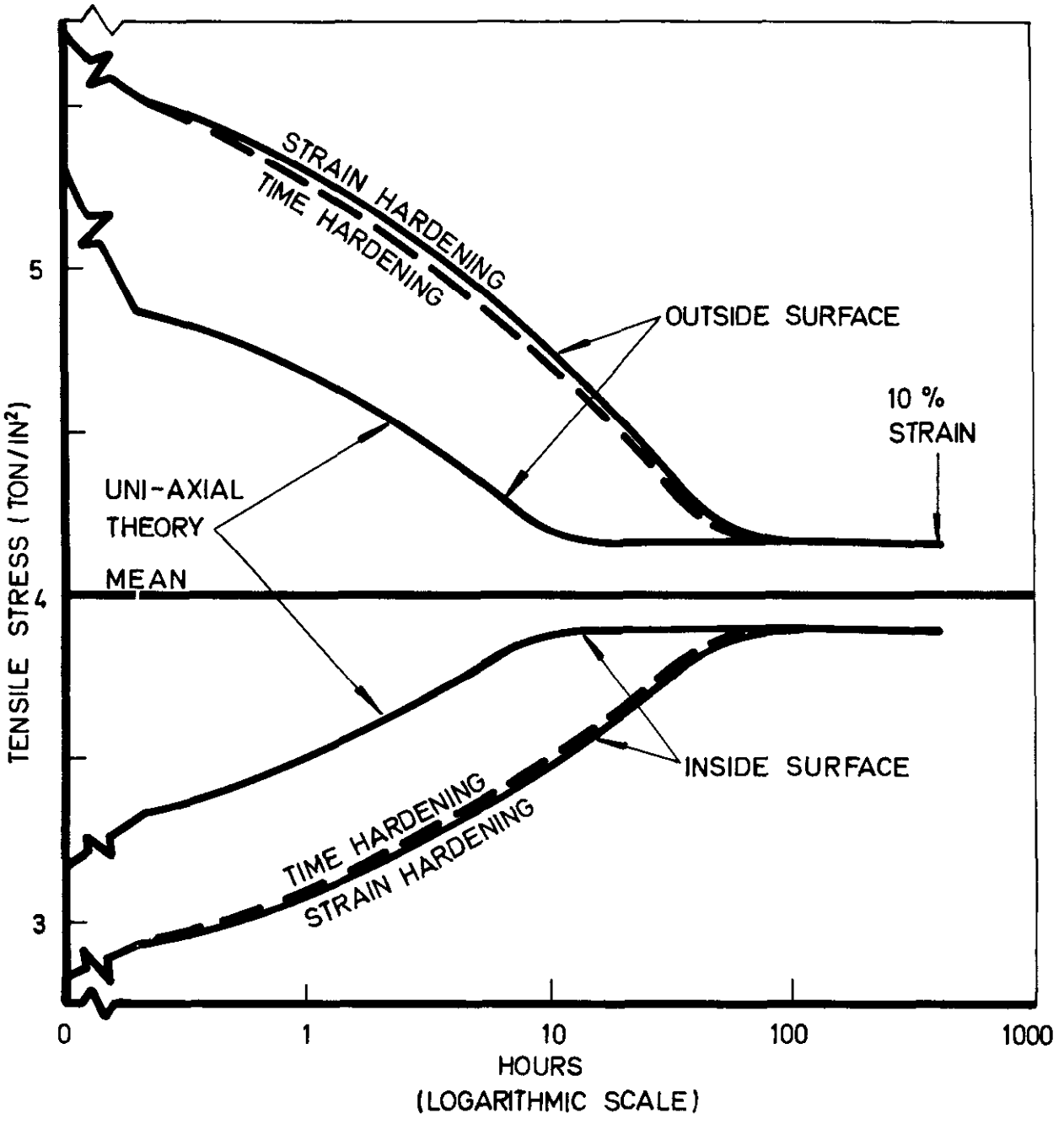

FIG 17 REDISTRIBUTION OF AXIAL STRESSES

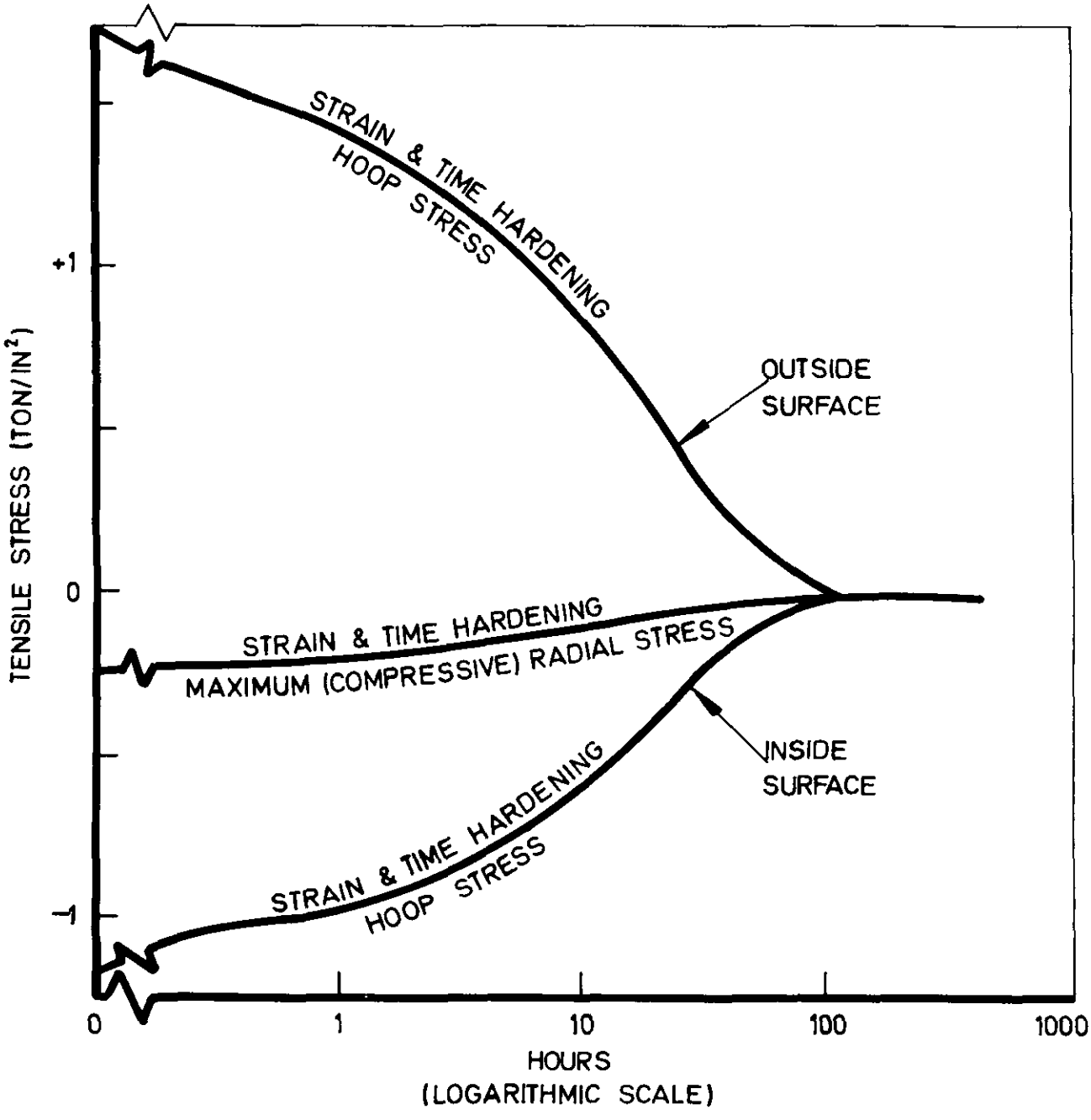

FIG 18 REDISTRIBUTION OF HOOP AND RADIAL STRESSES

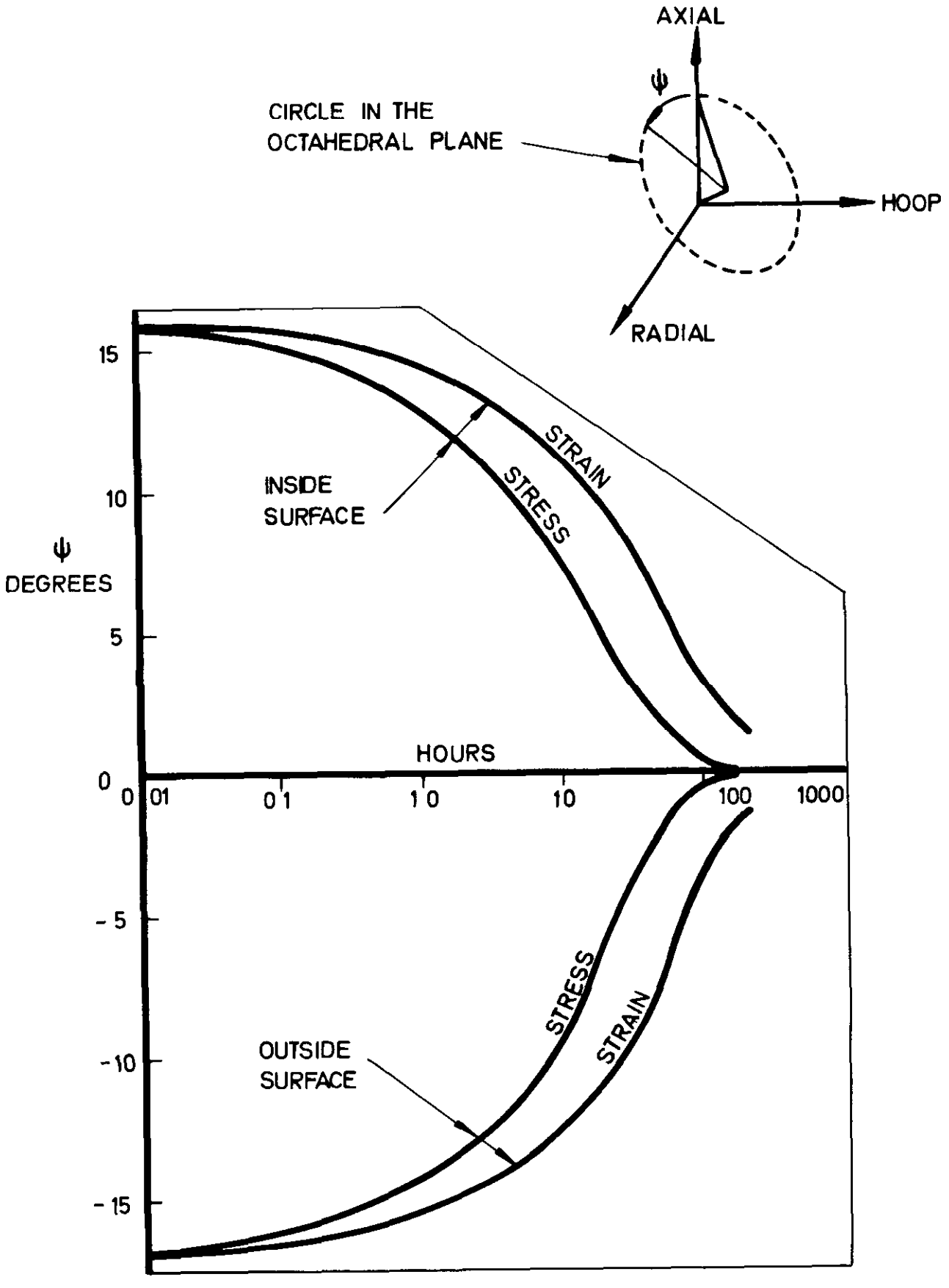

FIG 19 DIRECTIONS IN OCTAHEDRAL PLANE OF STRESSES AND CREEP STRAINS

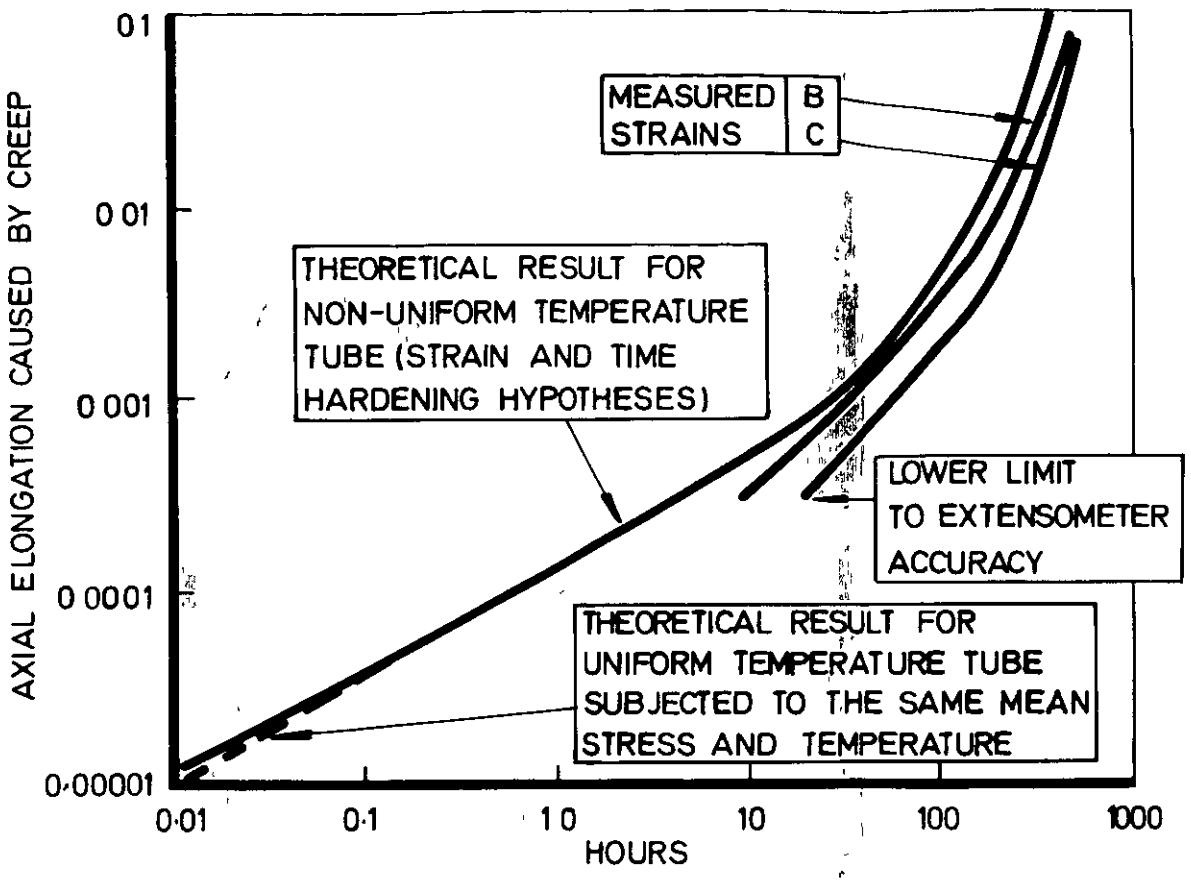

FIG 20 COMPARISON OF MEASURED AND CALCULATED ELONGATIONS

ARRANGEMENT TYPE	CODE	MEAN STRESS	RADIAL MEAN TEMPERATURE	STRAIN MEASURED	RUPTURE TIME
1	A	4 TON/IN^2	967·4 °C	NO	515 HR
1	B	4	967 4	YES	464
1	C	4	967·4	YES	485
2	D	4	967 4	NO	508
2	E	3 96	967 4	NO	515
3	F	4	970	NO	415
4	G	7	965	YES	33
4	H	7	965	YES	32
4	I	7	965	YES	38
4	J	4	970	YES	415
4	K	4	970	YES	374
4	L	4	970	YES	408
5	M	7	965	YES	34
5	N	4	970	NO	396

FIG 21 KEY TO RESULTS

A.R.C. C.P. No. 1024
June, 1967
Clarke, J. M.

539.434:539.319

AN INVESTIGATION OF STRESS REDISTRIBUTION CAUSED BY CREEP IN A THICK-WALLED CIRCULAR CYLINDER SUBJECTED TO AXIAL AND THERMAL LOADING

A thick-walled tube was subjected to an axial load and a radial temperature distribution which caused thermal stresses. The creep strains and the eventual rupture times were observed and compared with conventional creep tests and theoretical analysis. Theory suggested and experiments confirmed that stress redistribution caused the overall strain behaviour to approach that for the mean axial stress and the mean radial temperature.

Description of the experimental technique and apparatus includes a novel and simple optical extensometer. Appendices contain a complete analytic treatment of the triaxial stress problem in a long thick tube in

P.T.O.

A.R.C. C.P. No. 1024
June, 1967
Clarke, J. M.

539.434:539.319

AN INVESTIGATION OF STRESS REDISTRIBUTION CAUSED BY CREEP IN A THICK-WALLED CIRCULAR CYLINDER SUBJECTED TO AXIAL AND THERMAL LOADING

A thick-walled tube was subjected to an axial load and a radial temperature distribution which caused thermal stresses. The creep strains and the eventual rupture times were observed and compared with conventional creep tests and theoretical analysis. Theory suggested and experiments confirmed that stress redistribution caused the overall strain behaviour to approach that for the mean axial stress and the mean radial temperature.

Description of the experimental technique and apparatus includes a novel and simple optical extensometer. Appendices contain a complete analytic treatment of the triaxial stress problem in a long thick tube in

P.T.O.

A.R.C. C.P. No. 1024
June, 1967
Clarke, J. M.

539.434:539.319

AN INVESTIGATION OF STRESS REDISTRIBUTION CAUSED BY CREEP IN A THICK-WALLED CIRCULAR CYLINDER SUBJECTED TO AXIAL AND THERMAL LOADING

A thick-walled tube was subjected to an axial load and a radial temperature distribution which caused thermal stresses. The creep strains and the eventual rupture times were observed and compared with conventional creep tests and theoretical analysis. Theory suggested and experiments confirmed that stress redistribution caused the overall strain behaviour to approach that for the mean axial stress and the mean radial temperature.

Description of the experimental technique and apparatus includes a novel and simple optical extensometer. Appendices contain a complete analytic treatment of the triaxial stress problem in a long thick tube in

P.T.O.

the presence of an arbitrary distribution of non-elastic strains, and a treatment of some conditions under which stress-redistribution calculations can lead to a "steady state" or "fully redistributed" stress pattern.

A less rigorous theoretical treatment which ignores radial constraints is shown to lead to an under-estimate of the thermal stresses and of the time required for stress redistribution to occur.

the presence of an arbitrary distribution of non-elastic strains, and a treatment of some conditions under which stress-redistribution calculations can lead to a "steady state" or "fully redistributed" stress pattern.

A less rigorous theoretical treatment which ignores radial constraints is shown to lead to an under-estimate of the thermal stresses and of the time required for stress redistribution to occur.

the presence of an arbitrary distribution of non-elastic strains, and a treatment of some conditions under which stress-redistribution calculations can lead to a "steady state" or "fully redistributed" stress pattern.

A less rigorous theoretical treatment which ignores radial constraints is shown to lead to an under-estimate of the thermal stresses and of the time required for stress redistribution to occur.

Printed and published by
HER MAJESTY'S STATIONERY OFFICE

To be purchased from
49 High Holborn, London W.C 1
13A Castle Street, Edinburgh 2
109 St Mary Street, Cardiff CF1 1JW
Brazennose Street, Manchester M60 8AS
50 Fairfax Street, Bristol BS1 3DE
258 Broad Street, Birmingham 1
7 Linenhall Street, Belfast BT2 8AY
or through any bookseller

Printed in England

S O Code No 23 - 9018 - 24